Cell Systems

Classification and functional characterization of regulators of intracellular STING trafficking identified by genome-wide optical pooled screening

Highlights

- Performed genome-wide optical pooled screen to identify regulators of STING trafficking

- Mapped regulators of STING trafficking and signaling based on subcellular phenotypes

- OPS outperformed flow cytometry and fitness screens to resolve phenotypes

- Deorphaned C19orf25 and identified the HOPS and GARP complexes as STING regulators

Authors

Matteo Gentili, Rebecca J. Carlson, Bingxu Liu, ..., Yue Qin, Paul C. Blainey, Nir Hacohen

Correspondence

pblainey@broadinstitute.org (P.C.B.),
nhacohen@broadinstitute.org (N.H.)

In brief

Gentili et al. performed genome-wide optical pooled CRISPR screens to identify genes regulating trafficking and signaling of the innate immune sensor STING. Using machine learning, they clustered genes by phenotype, allowing them to deorphan a gene of unknown function (C19orf25) and identify the HOPS and GARP complexes as STING regulators.

CellPress

Cell Systems

Article

Classification and functional characterization of regulators of intracellular STING trafficking identified by genome-wide optical pooled screening

Matteo Gentili,[1,6] Rebecca J. Carlson,[1,2,6] Bingxu Liu,[1,6] Quentin Hellier,[1] Jocelyn Andrews,[1] Yue Qin,[1] Paul C. Blainey,[2,3,4,*] and Nir Hacohen[2,5,7,*]

[1]Broad Institute of MIT and Harvard, Cambridge, MA, USA
[2]Massachusetts Institute of Technology, Department of Health Sciences and Technology, Cambridge, MA, USA
[3]Massachusetts Institute of Technology, Department of Biological Engineering, Cambridge, MA, USA
[4]Koch Institute for Integrative Cancer Research at MIT, Cambridge, MA, USA
[5]Massachusetts General Hospital, Krantz Family Center for Cancer Research, Boston, MA, USA
[6]These authors contributed equally
[7]Lead contact
*Correspondence: pblainey@broadinstitute.org (P.C.B.), nhacohen@broadinstitute.org (N.H.)
https://doi.org/10.1016/j.cels.2024.11.004

SUMMARY

Stimulator of interferon genes (STING) traffics across intracellular compartments to trigger innate responses. Mutations in factors regulating this process lead to inflammatory disorders. To systematically identify factors involved in STING trafficking, we performed a genome-wide optical pooled screen (OPS). Based on the sub-cellular localization of STING in 45 million cells, we defined 464 clusters of gene perturbations based on their cellular phenotypes. A secondary, higher-dimensional OPS identified 73 finer clusters. We show that the loss of the gene of unknown function C19orf25, which clustered with USE1, a protein involved in Golgi-to-endoplasmic reticulum (ER) transport, enhances STING signaling. Additionally, HOPS deficiency delayed STING degradation and consequently increased signaling. Similarly, GARP/RIC1-RGP1 loss increased STING signaling by delaying STING Golgi exit. Our findings demonstrate that genome-wide genotype-phenotype maps based on high-content cell imaging outperform other screening approaches and provide a community resource for mining factors that impact STING trafficking and other cellular processes.

INTRODUCTION

The cyclic-GMP-AMP (cGAMP) synthase (cGAS)/stimulator of interferon genes (STING) pathway plays a key role in anti-pathogen defense, antitumor responses, neurodegenerative disease, and autoimmunity.[1] Mechanistically, cGAS-mediated cGAMP production in response to pathogen-derived double-stranded DNA (dsDNA) drives innate immune responses that are beneficial to the host. In addition, recognition of mislocalized self-DNA of nuclear or mitochondrial origin drives immunity against tumors.[2] Dysregulation of this pathway leads to disease, including the development of autoinflammatory and neurodegenerative disease due to steady-state or ligand-induced STING overactivation.[3,4]

Intracellular STING trafficking is essential for regulation of downstream responses. In the absence of ligand, STING is principally localized on the endoplasmic reticulum (ER) in the form of homodimers.[5] cGAMP binding to STING leads to oligomerization of the sensor, which in turn activates STING trafficking from the ER to the Golgi. STING is palmitoylated at the Golgi, leading to clustering and an increase in signaling,[6,7] and subsequent ubiquitination of the sensor.[8] STING then traffics to the *trans*-Golgi

network (TGN), where it interacts with TANK-binding kinase 1 (TBK1) to phosphorylate IRF3 and produce type I interferon (IFN).[7] Signaling shutdown is achieved by ESCRT-mediated degradation of ubiquitinated STING at the lysosome.[8–10] STING oligomerization has also been shown to drive autophagy activation, an ancestral activity of the pathway important in pathogen clearance.[11] Activation of STING-dependent non-canonical autophagy and the inflammasome relies on a channel formed in the transmembrane domain of STING dimers, leading to pH imbalance in the Golgi compartment.[12,13] Finally, STING has also been shown to activate the nuclear factor κB (NF-κB) pathway to induce pro-inflammatory cytokines, even though the mechanism is less clear.[14]

In addition to cyclic di-nucleotide-mediated trafficking, we and others have shown that cGAS basal activity primes STING, leading to a homeostatic degradative flux, and post-Golgi interruption of this flux leads to spontaneous activation of the sensor.[8,15] This is a process of particular physiological relevance since mutations in genes regulating STING trafficking have been found in patients with autoinflammatory diseases. Mutations in the COPI subunit COPA found in patients with COPA syndrome lead to STING accumulation at the Golgi, resulting in autoinflammation in

patients.[16–20] Similarly, mutations in two genes driving neurodegenerative diseases, C9orf72 for amyotrophic lateral syndrome (ALS) and NPC1 for Niemann-Pick disease, impair STING degradation at the lysosome, inducing heightened or constitutive STING-dependent responses and resulting in disease.[21,22] Maintaining homeostasis of the STING pathway is therefore central to avoiding exacerbated activation of inflammatory responses. On the other hand, blocking STING degradation has been shown to be beneficial in the context of antitumor immunity since STING-dependent type I IFN, central to activation of the immune system against tumors, can be boosted.[15,23] Understanding regulators of STING trafficking is therefore important both in the context of autoinflammation and antitumor immunity.

In order to identify genes regulating STING trafficking, we previously performed flow-based CRISPR screens and proximity-ligation proteomics that led us to characterize ESCRT as a regulator of STING degradation at the endosome.[8] The screen used a terminal readout of STING degradation at the lysosome, but STING trafficking is a dynamic and multifaceted process that can be followed intracellularly via microscopy. Here, we set out to associate genetic perturbations with specific intracellular trafficking phenotypes upon STING activation. To achieve this goal at the genome-wide level, we took advantage of optical pooled screens (OPS),[24] a method for simultaneous single-cell imaging of cellular phenotypes and readout of single guide RNA (sgRNA) sequences, thus enabling high-throughput image-based pooled genetic screens in millions of cells.[25,26] Briefly, in OPS, cells are transduced with perturbation libraries, and image-based phenotypes are acquired. Following phenotyping, in situ sequencing is performed to determine the identity of the perturbations in each cell. Finally, phenotyping and sequencing images are aligned to enable assignment of single-cell perturbation identities with phenotypic profiles. We show that OPS outperforms previous STING screens relying on one-dimensional flow cytometric or fitness readouts using a meta-analysis approach.[27] In addition, this high-content screen allows for further interpretation directly from screening data. Using dimensionality reduction and unsupervised clustering based on image-based phenotypes,[25,26,28] we identify groups of genes that similarly affect STING trafficking when knocked out, and we show that this dataset is useful for assigning functional roles to previously uncharacterized genes. We focused on two groups of genes regulating STING degradation at distinct stages and found that the homotypic fusion and protein sorting (HOPS) complex is required for signaling shutdown at the endolysosome. Similarly, we show that the Golgi-associated retrograde protein (GARP) complex subunit VPS52 and the RAB6 Guanine nucleotide exchange factor (GEF) RIC1/RGP1 complex drive STING degradation by promoting its exit from the Golgi. Overall, by performing high-content OPS, we provide a resource to the community to guide the identification of genes regulating STING biology.

RESULTS

A genome-wide optical pooled screen efficiently retrieves genes involved in STING trafficking

In order to identify genetic regulators of STING subcellular trafficking, we performed an optical pooled screen (OPS) in HeLa-TetR-Cas9 cells (Figure 1A).[29] HeLa cells were transduced with STING-mNeonGreen (mNG) to monitor STING localization and flow sorted twice to select for cells with similar reporter expression levels. Cells were transduced with a library of sgRNAs targeting ~20,000 genes with 4 sgRNAs/gene, along with 454 non-targeting sgRNAs (ntgRNAs) previously described.[25] Cas9 was induced for 7 days with doxycycline. Following library transduction and doxycycline treatment, cells were replated on glass-bottom dishes (for imaging) and stimulated with cGAMP for 4 h. Cells were stained for nuclei (DAPI) and markers of subcellular compartments involved in STING trafficking (Golgi, GM130; endolysosomes, CD63) and p62, an autophagy receptor that accumulates in response to STING activation and has been shown to interact with STING[30] (Figure 1B). As expected, cGAMP induced STING translocation from the ER to the Golgi apparatus and endolysosomal compartments (Figure 1B). In order to assess perturbation-induced changes in the distribution and degradation of STING, we also acquired images on cells transduced with the pool of 454 ntgRNAs (1) without cGAMP treatment, (2) 4 h post cGAMP stimulation (the screen time point), and (3) 5 h post cGAMP stimulation.

Following imaging and in situ sequencing of 45 million cells with 80,000 perturbations (Figure S1A), we defined the phenotype of each cell based on thousands of features extracted from the images, including intensity, marker colocalization, subcellular variation, texture, and shape (using CellProfiler,[31] scikit image,[32] and mahotas[33]) (Table S1). Using all features derived from the STING or p62 channels (Figure S1B) and including information from other channels such as colocalization with CD63 or GM130, we developed three independent linear support vector machine (SVM) classifiers (Table S2) to determine which 4-h stimulated cells in the screen displayed three distinct phenotypes (Figure 1C). We trained one SVM per perturbation on the task of distinguishing cells that received the perturbation of interest from non-targeting control cells. We used an 80/20 train test split and determined a score based on the prediction on held-out perturbed cells from the test set (a score of 1 indicating all perturbed cells were correctly classified as perturbed while a score of 0 indicating all cells were classified as unperturbed) (Figure 1D). In addition to this unbiased classifier, we also trained two additional linear SVM classifiers to distinguish either unstimulated non-targeting control cells vs. stimulated control cells at the screen time point (4 h) (Figure 1E) or non-targeting control cells from the screen time point vs. non-targeting control cells stimulated for 5 h (Figure 1F). One classifier allowed us to identify perturbations that led to states similar to those of control unstimulated cells, identifying 194 genes required for STING exit from the ER/Golgi ("unstimulated" classifier; Figures 1E and S1C); the other classifier found perturbations similar to control cells at 5 h post cGAMP, finding 133 genes that may accelerate STING trafficking or lead to STING accumulation in the endolysosomal compartment ("stimulated" classifier; Figures 1F and S1C). These two latter classifiers identified genes not found by the first classifier (Figure 1G), likely because of increased power for detecting specific stimulation conditions thanks to classifier training and feature selection on these conditions. The classifiers reported known genes: for instance, SEC24C, which is critical for STING exit from the ER[11] and should therefore result in cells appearing unstimulated when knocked out, was one of the top 5 hits in the unstimulated classifier and also a hit in the perturbed
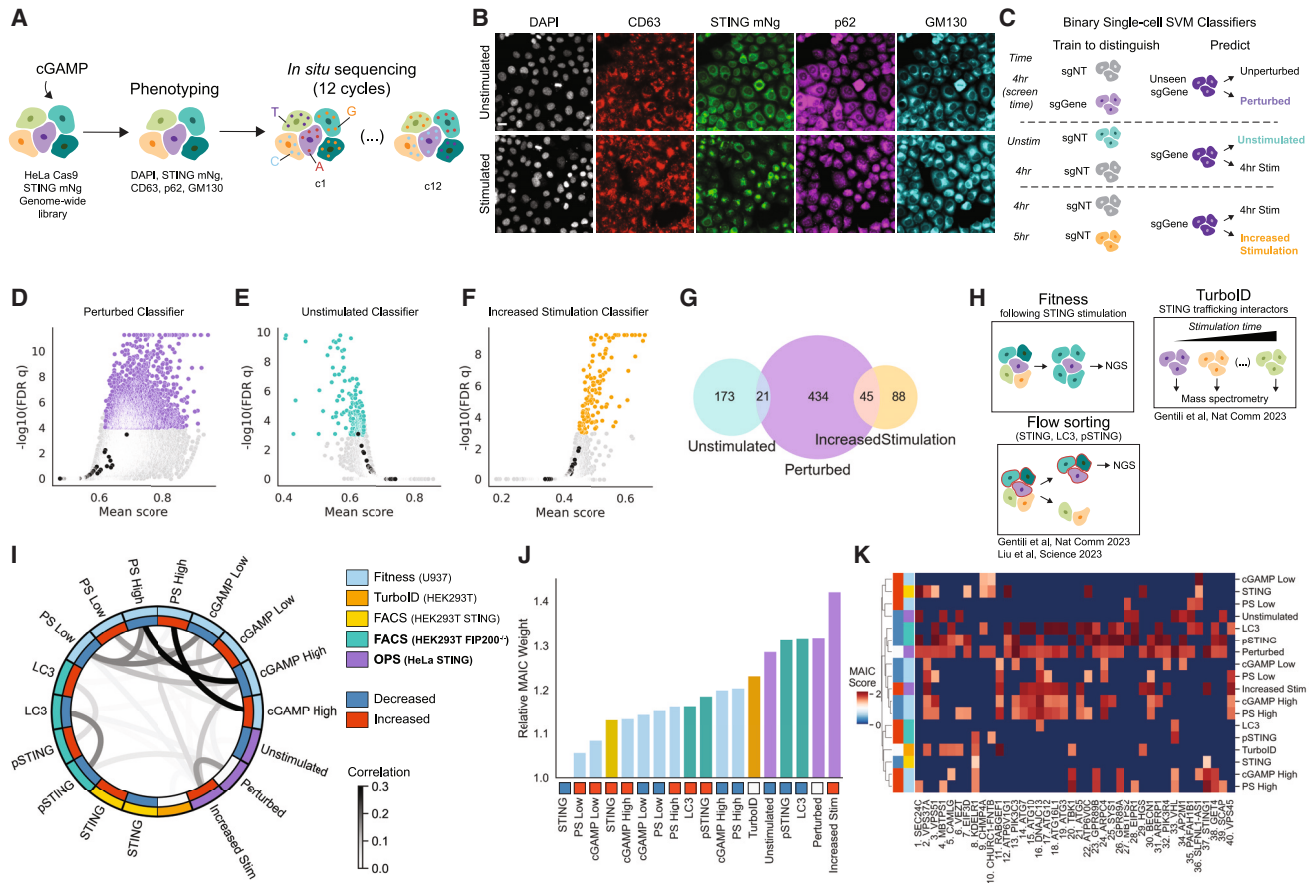
Figure 1. A genome-wide optical pooled screen identifies genes regulating STING trafficking
(A) Genome-wide optical pooled screening workflow.
(B) Example fields of view of HeLa cells from the optical pooled screen either unstimulated (top) or stimulated (bottom) with cGAMP for 4 h. Scale bar, 20 μm.
(C) Schematic of single-cell support vector machine (SVM) classifiers used to call hits from the genome-wide optical pooled screen using features from the p62 and STING channels. 4 h indicates cGAMP-stimulated cells that received the genome-wide KO library. 5 h refers to control cells with non-targeting sgRNAs stimulated with cGAMP for 5 h.
(D–F) Volcano plot of hits from the perturbed vs. unperturbed classifier (D), unstimulated classifier (E), and increased stimulation classifier (F). Black dots indicate individual non-targeting sgRNAs.
(G) Venn diagram showing overlap of top 500 significant hits from each classifier.
(H) Genome-wide fitness and flow cytometry screening outlines and mass spectrometry STING interaction screen.
(I) Chord diagram showing Pearson correlation between MAIC scores for the top 500 significant hits from each of the STING datasets. Same experimental batch performed on the same day highlighted by the same color in the outer ring.
(J) Weighting score for each of the STING datasets provided by the MAIC algorithm. The weighting score given to a dataset is proportional to the average score of the genes belonging to this dataset, and genes appearing in multiple datasets score more highly.
(K) Scores for each of the top 40 genes in each screening condition.

classifier, but not in the increased stimulation classifier. On the other hand, VPS37A, which results in increased STING accumulation when knocked out,[8] was one of the top 15 hits in the increased stimulation classifier and scored in the perturbed classifier but not in the unstimulated classifier. In total, the optical screen identified 695 gene hits at adjusted false discovery rate [FDR] ≤ 0.1% (Benjamini-Hochberg) in at least one model.

We next combined the results of the optical screen with other non-imaging-based genome-wide genetic screens that we carried out to find regulators of STING activation (Figure 1H). Four screens in total were used in this analysis. Two screens were previously published that identified regulators of STING trafficking[8] and STING-dependent LC3B lipidation[12] in HEK293T.

Two screens are reported here for the first time (Table S3). The first one uses STING-dependent cell death as a readout. We stimulated U937 cells with a high dose of cGAMP to induce STING-dependent cell death and quantified sgRNA enrichment 48 h after stimulation. The second one identifies regulators of STING phosphorylation. We used HEK293T STING-hemagglutinin (HA) cells FIP200 knockout (KO) to reduce background levels of canonical autophagy, described in Liu et al.,[12] stimulated with cGAMP, and performed intracellular staining with a phospho-STING antibody. Sorting was used to separate phospho-STING-positive and -negative cells, and sgRNA enrichment was quantified in the sorted populations (Figures 1H and S1E). To complement these genetic screens, we also included 132

genes encoding proteins that we found in physical proximity to STING at 4 time points after activation using proximity-ligation proteomics.[8]

In order to integrate results from these diverse sources, we turned to meta-analysis by information content (MAIC), a previously published algorithm for combining data from diverse sources of unknown quality.[27] Briefly, MAIC takes as input ranked or unranked gene lists from multiple experiments and produces a weighting factor for each list based on overlap with the other lists provided; these weights are then used to calculate a final score for each gene. We examined the correlation of hit genes across the optical screen and these genetic and proteomic studies (Figure 1I). In addition to higher Pearson correlations of relative MAIC[27] scores for screens performed at the same time, we observed that genes for which KO increased cell death were correlated with genes found in the increased stimulation classifier, while those that decreased cell death, pSTING, or STING intensity levels by flow cytometry were often included in our perturbed classifier. Using our previously described MAIC approach to compare the power of each screen to find likely true positives (across 18 gene lists and 9 screens), the top two performers were optical pooled screening classifiers (increased stimulation and perturbed), and the remaining OPS classifier—unstimulated—was ranked 5th (Figure 1J). Therefore, despite the high quality of the previous datasets that revealed several new STING regulators and functions,[8,12] our high-content image-based OPS dataset resulted in more informative gene lists than previous approaches. By integrating multiple screens performed in distinct biological models, we developed a consensus list of 1,225 genes that scored in at least two distinct screens (Table S4), yielding increased confidence in the broad biological relevance of these genes to the STING pathway. Indeed, even among the top 40 genes, many of which are well-established regulators of the STING pathway, no gene scored in all screening settings (Figures 1K and S1D), revealing the importance of dataset integration for prioritization of high-confidence genes.

Unsupervised clustering and dimensionality reduction reveal genes with similar effects on STING trafficking

We further explored the biological functions of these 1,225 consensus genes by performing unsupervised analyses on the image-based features obtained from our high-content genome-wide optical pooled screen. To do this, we performed dimensionality reduction on thousands of gene-level mean features using the PHATE algorithm[34] and performed Leiden clustering[35] to identify 464 clusters of genes of interest (Figures S2A; Figure S2A). To further infer the functions of genes in these clusters, we identified clusters that were enriched for hits derived using our unstimulated classifier (Figure 2A). Among the clusters that scored as significant, cluster 1 included a number of ER membrane genes, including two known regulators of STING ER exit, SEC24C[11] and SCAP,[36] as well as other ER-localized genes not yet shown to regulate STING such as MBTPS1 and MBTPS2 that were recently reported to act with SCAP to regulate NF-κB.[37] We also observed a cluster of dynein/dynactin factors (cluster 18); these complexes have previously been associated with ER exit but not shown to be required for STING activation.[38] Finally, we observed that the GARP complex delayed STING activation at a later stage,

causing cells to look significantly more like unperturbed cells at 4 h than unperturbed cells at a longer 5 h stimulation time point.

To test if the hits identified in our screens impacted transcription in resting cells, potentially pointing to perturbation effects acting indirectly on STING, we integrated our dataset with the genome-scale Perturb-seq dataset.[39] By doing so, we identified very few clusters with enrichment (clusters 15, 71) for perturbations that led to hits in the genome-scale Perturb-seq screen with significant differentially expressed genes (Figures 2B and S2C), increasing confidence that many of our hits do not affect general cellular processes and likely have a direct impact on STING trafficking. To further increase confidence in our clustering approach, we tested whether clusters at a significant distance from the ntgRNAs were enriched for protein-protein interactions (PPIs) as defined in the Comprehensive Resource of Mammalian Protein Complexes (CORUM) dataset[40] and confirmed that mean distance from ntgRNAs positively correlated with an enrichment in PPIs (Figure S2D). Additionally, clusters containing more than one gene and less than 20% ntgRNAs showed significant enrichment for Gene Ontology (GO), Reactome, Kyoto Encyclopedia of Genes and Genomes (KEGG), CORUM, and Jensen terms (Figure S2E). This confirmed that our clustering approach identified biologically related groups of genetic perturbations.

Next, we identified clusters of genes that were enriched for genes with increased stimulation in our classifier (Figure 2C). These include a cluster containing SURF4, a protein that when knocked out results in increased accumulation of STING at the Golgi,[18] the HOPS complex, and several clusters related to autophagy (5, 11, and 13). In fact, when examining two distinct stages of autophagy, initiation, and conjugation, we found that our screen identified the majority of genes critical for these stages and that they clustered separately as cluster 5 (orange) and cluster 13 (purple) (Figures 2D and 2E), mostly based on intensity and texture features from both the STING and p62 channels. Single-cell images indeed revealed distinct patterns for p62 and STING for autophagy initiation and conjugation factors (Figure 2F). Notably, EI24, a gene involved in autophagy that was only recently revealed to be involved in initiation, clustered with other canonical initiation factors.[41] We therefore experimentally confirmed that EI24 KO significantly affects STING signaling by knocking out this gene in hTERT-immortalized primary BJ1 fibroblasts. Via western blotting, we observed an increase in LC3B lipidation, a reduction in STING degradation, and a consequent increase in pSTING and pTBK1 downstream signaling, suggesting that, like ATG9A, which clustered with EI24 (Figures 2C and 2D) and was shown to regulate STING trafficking,[42] EI24 is involved in STING signaling shutdown (Figures 2G and S2F).

Secondary screens further characterize genes involved in STING trafficking and signaling

To further confirm the effect of 262 top genes involved in STING trafficking, we performed follow-up screening in HeLa cells (Table S6) and BJ1 fibroblasts (Table S7), thus diversifying the cellular models studied (Figures 3A–3C). We imaged at higher resolution in (1) time, with unstimulated, 4 h, and 6 h post cGAMP treatment for HeLa, and 4 h for BJ1 and (2) phenotype, by expanding to 11 imaging channels using the iterative immunophenotyping method 4i in HeLa[43] (Figures 3A–3C). We visualized
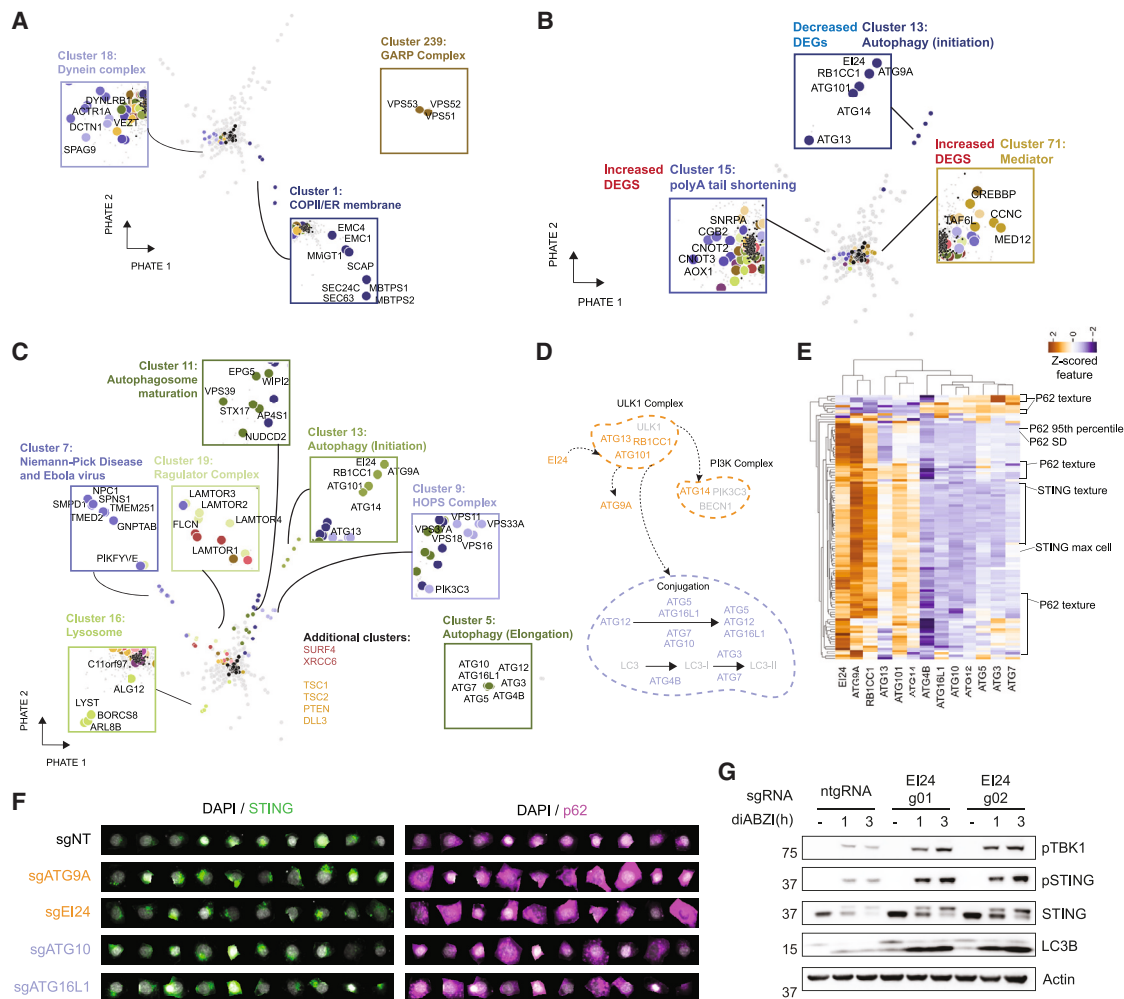
Figure 2. Unsupervised clustering identifies groups of genes that similarly affect STING trafficking

(A) PHATE plot of 1,225 consensus genes highlighting top clusters significantly enriched for genes that are less stimulated because they are either more similar to unstimulated non-targeting control cells (clusters 1, 18—unstimulated classifier) or significantly more similar to non-targeting control cells at 4 h than at 5 h (cluster 239).

(B) PHATE plot of consensus genes highlighting clusters significantly enriched for genes that have a high or low number of differentially expressed genes in the genome-scale Perturb-seq dataset.

(C) PHATE plot of consensus genes highlighting top clusters significantly enriched for genes that are more stimulated than non-targeting control cells (increased stimulation classifier).

(D) Autophagy diagram highlighting genes identified in cluster 13 (orange) or 5 (purple).

(E) Hierarchically clustered heatmap (clustered using seaborn clustermap with method: "average," metric: "Euclidean"), showing features differentiating genes from the two autophagy clusters in (D).

(F) Single-cell images of STING and p62 channels randomly selected from non-targeting controls and KO of selected autophagy factors from the genome-wide OPS.

(G) Immunoblot of the indicated proteins in control (ntgRNA) or EI24 KO BJ1 fibroblasts stimulated with 1 μM diABZI for the indicated times. One representative blot of n = 3 independent experiments.

proteins relevant to STING signaling (STING, NF-κB p65, p62), STING trafficking compartments (calnexin [CANX] in the ER, GM130 in Golgi, EEA1 in endosomes), STING degradation (HGS, ATP6V1D), and cell state (DAPI/nuclei, actin, γH2AX) (example images for all channels in Figure S3A). As with the genome-wide screen, we extracted thousands of features from each channel without background subtraction as well as with the addition of a rolling ball background subtraction step (Figures 3C and S3A).[44] In HeLa cells, STING colocalization

with CANX decreased after stimulation with cGAMP, while STING colocalization with GM130, HGS, and EEA1 increased (Figure S3B). Additionally, the NF-κB subunit p65 showed increased signal intensity in DAPI-positive nuclei upon cGAMP stimulation (Figure S3B). These results recapitulated the expected responses and served to technically validate the 4i stainings.

We identified factors affecting STING activation and degradation in both cell types based on pSTING and STING intensity
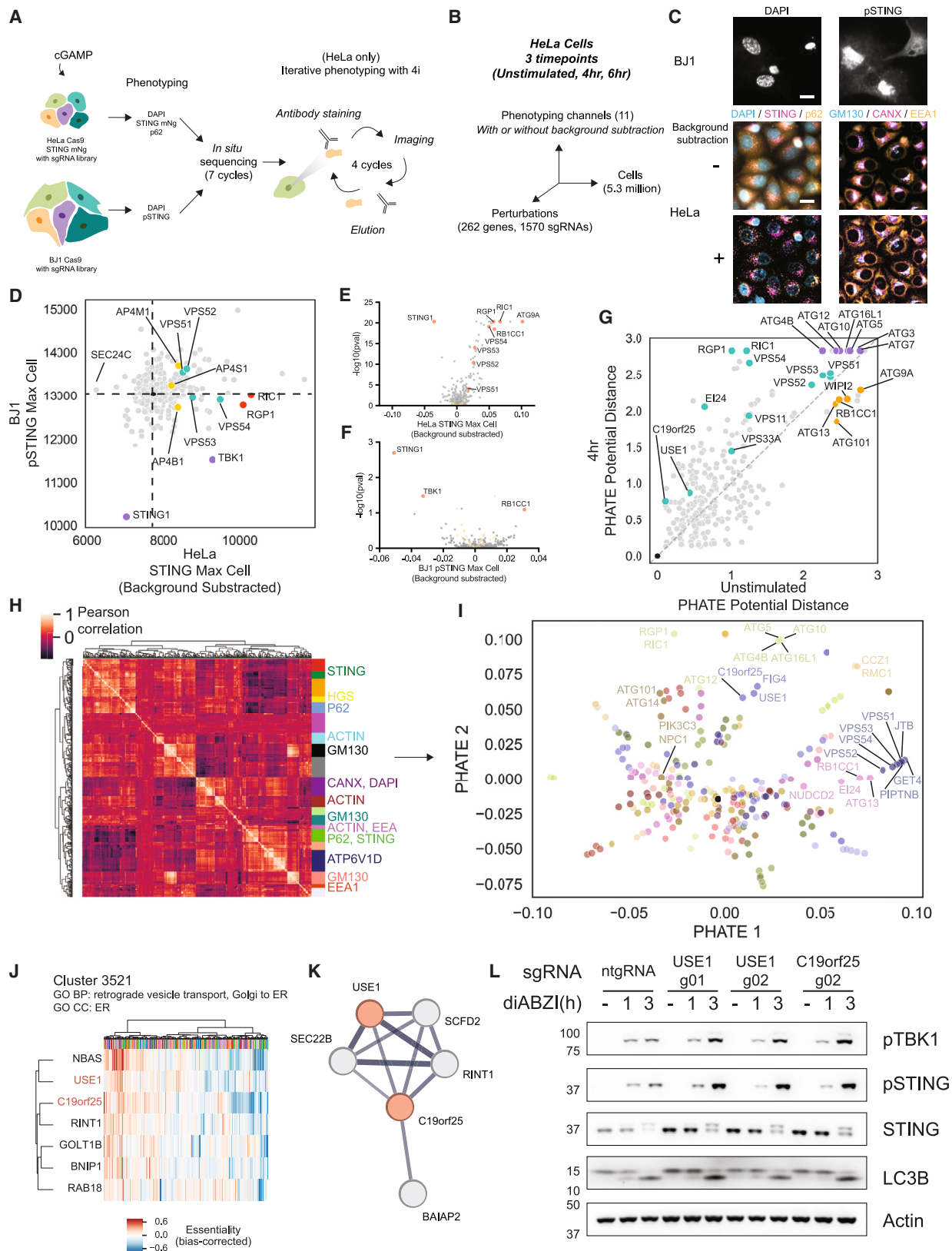
(Figures 3D–3F). We then calculated the change in phenotype (relative to ntgRNAs) after dimensionality reduction of all features in cells that are unstimulated or after 4 h of cGAMP treatment (Figure 3G), aiming to prioritize genes with fewer morphological effects in the unstimulated condition. For example, we saw that factors involved in autophagy conjugation, a process required for both canonical autophagy and STING-induced Conjugation of ATG8 on Single Membranes (CASM),[46,47] were more cGAMP-specific than upstream autophagy initiation factors required only for canonical autophagy (Figure 3G). Next, we performed feature clustering to identify 20 modules of co-regulated features (Figure 3H) in order to equalize the weights of feature types given the large number of channels and features in this screen and performed potential of heat-diffusion for affinity-based trajectory embedding (PHATE) dimensionality reduction and Leiden clustering on mean per-gene values across these feature modules (Figures 3I and S3C; Table S8). This approach enables better-distributed weighting of orthogonal feature groups.

By identifying genes in close proximity in the reduced dimensional space and focusing on perturbations that impact the stimulated more than the unstimulated phenotype (Figure 3G), we observed that the poorly characterized gene C19orf25 co-clustered with USE1, a better-characterized ER membrane protein involved in Golgi-ER retrograde transport[48] (Figure 3I). USE1 was found proximal to STING in non-stimulated cells by proximity-ligation proteomics[8] (Figure S3D). To confirm the association of C19orf25 with USE1 and STING, we examined clustering of co-essential modules from genome-wide fitness screens across cell types and observed again that C19orf25 was in the same cluster as USE1 in several instances, including cluster 3,521, which contained genes related to retrograde Golgi-ER transport[45] (Figure 3J). Additionally, we used the Search Tool for the Retrieval of Interacting Genes/Proteins (STRING) physical interaction subnetwork[49] and observed that USE1 was one of five medium-confidence proteins that physically interacted with C19orf25 in immunoprecipitation assays (interaction score 0.582) (Figure 3K). Analysis of deviation from ntgRNAs in the secondary screen showed that KO of both USE1 and C19orf25 led to increased STING colocalization with Golgi (GM130) and auto-

phagy (p62) markers (Figure S3E). Additionally, consistent with a role of USE1 in Golgi-to-ER recycling, KO of USE1 in non-stimulated cells led to an increase of STING colocalization with GM130, while KO of C19orf25 led to an increase in STING colocalization with CANX (Figure S3F), suggesting that these genes, similar to COPA,[16–18,20] play a role in STING Golgi-to-ER recycling. We further experimentally confirmed that knocking out C19orf25 and USE1 in BJ1 fibroblasts indeed leads to an increase in STING, pSTING, and pTBK1, consistent with the hypothesis that both genes are involved in retrograde Golgi-ER transport of proteins such as STING (Figure 3L). Through optical pooled screening and integration of other datasets, we therefore inferred a biological function for C19orf25 and confirmed its role in regulation of STING activation.

We next focused on three complexes that have not been previously associated with STING trafficking and which have genetic mutations associated with disease in the human population: the HOPS complex, the GARP complex, and the RIC1-RGP1 complex (Figure S3G).

The HOPS complex subunits VPS11 and VPS33A regulate STING degradation at the lysosome

We next examined the impact of KO of the HOPS complex on STING trafficking and signaling, as the HOPS complex was not previously described to regulate STING degradation. This complex regulates membrane fusion in the endolysosomal compartment and has been shown to drive membrane fusion between autophagosomes and lysosomes.[50] Additionally, mutations in the VPS11 and VPS33A subunits of the complex have been found in patients with neurodegenerative diseases.[51,52]

Results from the genome-wide screen showed that the HOPS complex subunits VPS11, 33A, 18, and 16 clustered together (Figure 2C) and increased STING max (max intensity of STING pixels) and mad (median absolute deviation of STING pixels) in the cytoplasm when knocked out (Figures S4A and S4B). In the genome-wide screen, the endosomal sorting complex required for transport (ESCRT) subunit VPS37A, which we showed regulates STING degradation in the endolysosomal compartment,[8] clustered with the HOPS complex (Figures 2C), suggesting that the phenotype described in VPS37A KO cells

Figure 3. Secondary screens with additional dimensions further characterize genes regulating STING trafficking
(A) Workflow for targeted follow-up STING screens.
(B) HeLa secondary screen is high-dimensional along multiple axes.
(C) Selected fields of view from secondary screens for BJ1 cells and HeLa cells with or without background subtraction. Scale bar, 20 μm.
(D) Scatterplot of secondary screen per-gene mean STING maximum (per cell) in HeLa cells compared with pSTING maximum per cell in BJ1 fibroblasts, and black dot at the center of the dashed lines indicates non-targeting controls. Each point represents the average of measurements for each of the 262 targeted genes.
(E and F) (E) Volcano plot of mean STING maximum (per cell) in HeLa cells (deviation from ntgRNAs) and (F) pSTING maximum (per cell) in BJ1 fibroblasts (deviation from ntgRNAs), and yellow dots indicate non-targeting control sgRNAs. Each point represents the average of measurements for the STING intensities on the x axis and the Stouffer aggregated p values on the y axis each of the 262 targeted genes.
(G) Correlation between phenotype (calculated as PHATE distance relative to NT sgRNAs) for each perturbed gene in the unstimulated vs. 4 h cGAMP-stimulated condition.
(H) Hierarchical clustering based on Euclidean distance of HeLa screen features into 20 distinct modules. Clusters containing at least 40% of features related to a given channel are annotated.
(I) PHATE dimensionality reduction and Leiden clustering of secondary screen genes using as input mean per-gene scores across the 20 modules identified in (G).
(J) Cluster 3521 and significant Gene Ontology (GO) terms as previously described.[45] x axis indicates distinct cell lines. C19orf25 and USE1 are manually highlighted.
(K) STRING v11.5 physical subnetwork potential interactions (minimum score = 0.4) with C19orf25; USE1 and C19orf25 are manually highlighted.
(L) Immunoblot of the indicated proteins in control (ntgRNA) or USE1 or C19orf25 KO BJ1 fibroblasts stimulated with 1 μM diABZI for the indicated times. One representative blot of n = 3 experiments.
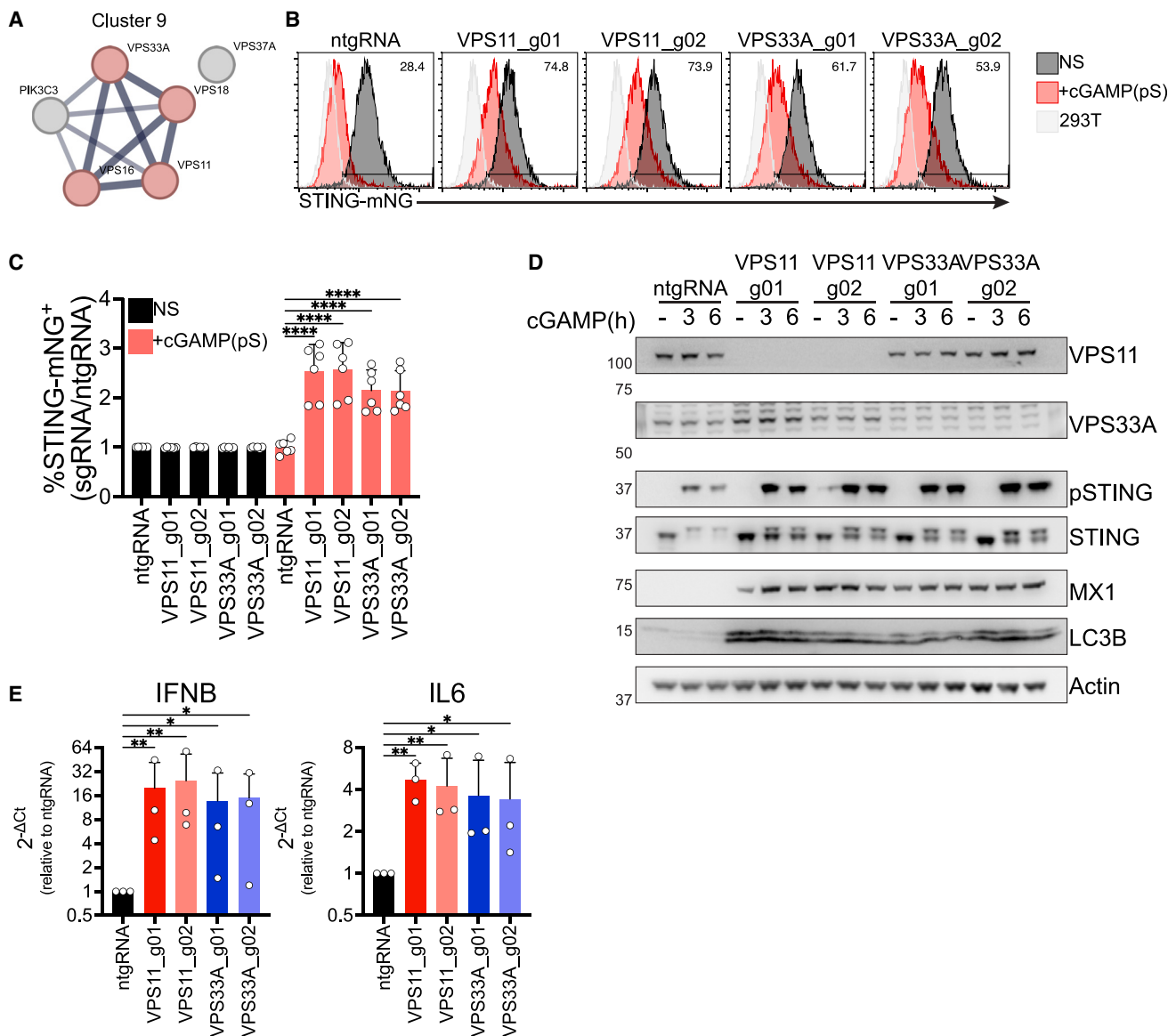
A Cluster 9

B

STING-mNG

NS
+cGAMP(pS)
293T

C

D

E

Figure 4. The HOPS complex subunits VPS11 and VPS33A are required for STING degradation

(A) STRING network of interaction of the indicated proteins found in cluster 9 of the dimensionality reduced data shown in Figure 2.

(B) mNG levels in 293 T STING-mNG cell lines KO for the indicated genes stimulated with 4 μg/mL 2'3'-cGAMP(pS)2 (in medium) for 6 h. One representative plot of n = 3 independent experiments with n = 2 technical replicates per experiment.

(C) Percentage of STING-mNG-positive cells in cells stimulated as in (B).

(D) Immunoblot of the indicated proteins in BJ1 fibroblasts transduced with a control guide (ntgRNA) or with VPS11 or VPS33A sgRNAs and stimulated with 0.5 μg/mL cGAMP (in perm buffer) for the indicated times.

(E) qPCR for IFNβ (left) and IL-6 (right) in BJ1 fibroblasts KO for VPS11 (red) or VPS33A (blue) stimulated with 0.5 μg/mL cGAMP (in perm buffer) for 6 h. n = 3 independent experiments. $2^{-\Delta Ct}$ fold change calculated as ratio $2^{-\Delta Ct}$ sgRNA/$2^{-\Delta Ct}$ ntgRNA for cells stimulated with cGAMP. One-way ANOVA on log-transformed data with Dunnet multiple comparison test.

In all panels, bar plots show mean and error bars standard deviation. Marker unit for western blots is kDa. $*p < 0.05, **p < 0.01, ***p < 0.001, ****p < 0.0001$; ns, not significant.

could be similar to HOPS complex KO. The subunits in cluster 9 of the genome-wide screen (Figure 4A) are shared between the HOPS and the class C core vacuole/endosome tethering (CORVET) complex.[53] We excluded CORVET since VPS3 and VPS8 did not score in the genome-wide screen, while VPS39 and VPS41, which are part of the HOPS complex, were found

to increase STING mad upon KO, and VPS39 was found in cluster 11 (Figure 2C). To test if the HOPS complex plays a role in STING degradation, we knocked out VPS11 and VPS33A in a STING- mNG reporter line we previously described[8] (Figure S4C). This 293T reporter line expresses STING fused to mNG, allowing us to quantify STING degradation upon
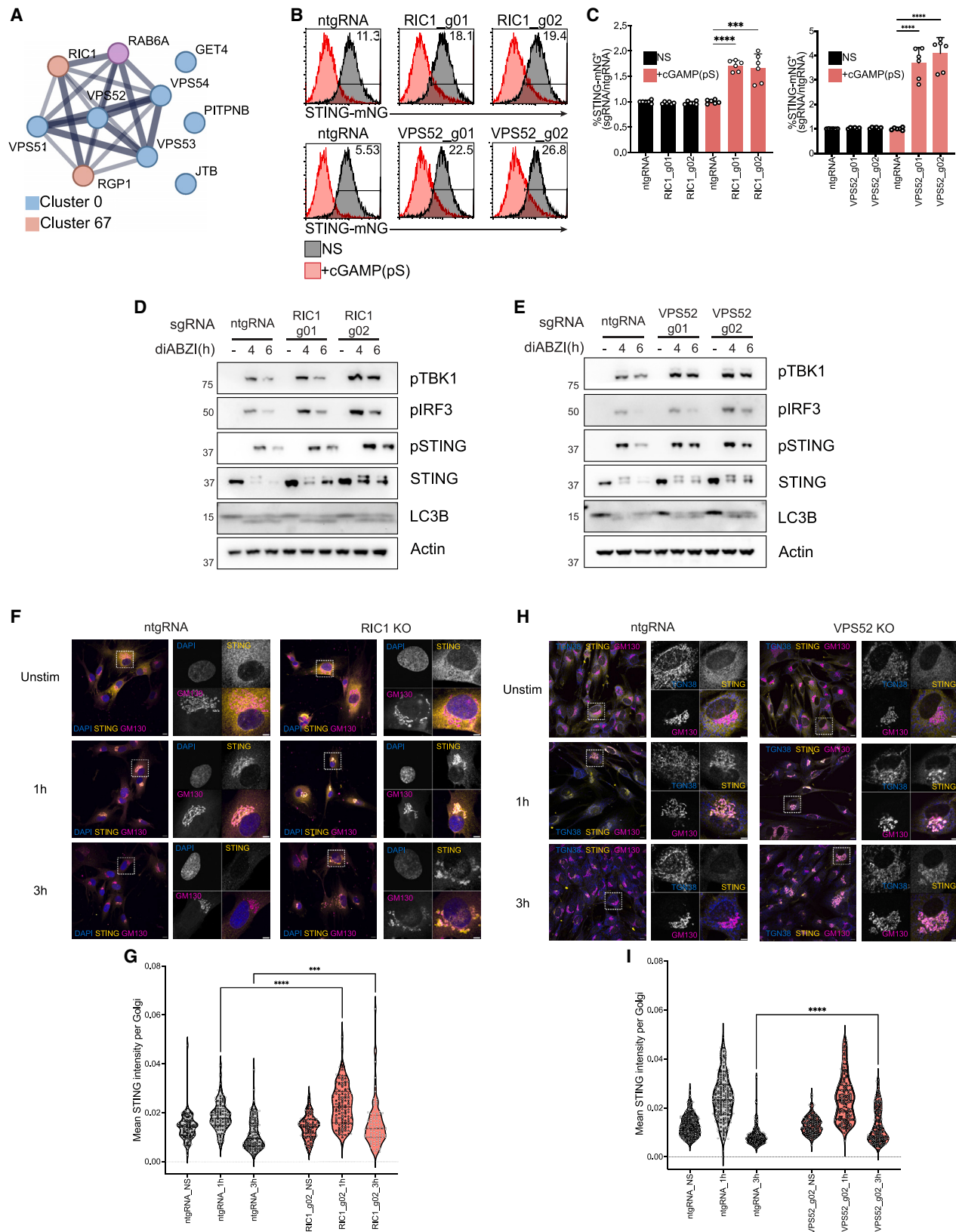
stimulation with the cGAMP stable homolog cGAMP(pS)2 via flow cytometry. KO of either subunit of the HOPS complex led to a reduction in STING degradation (Figures 4B and 4C). We then tested the impact of VPS11 or VPS33A KO on STING signaling by knocking out either subunit with two independent sgRNAs in BJ1 fibroblasts. VPS11 or VPS33A KO led to a reduction in STING degradation, consistent with our screens and our reporter line, and increased STING phosphorylation both at 3 and 6 h post-stimulation with cGAMP (Figure 4D), resulting in increased expression of IFN-β and interleukin (IL)-6 (Figures 4E and S4D). As expected, KO of either HOPS subunit led to a defect in autophagic flux, as shown by the accumulation of lipidated LC3B at steady state in the absence of ligand (Figure 4D). Interestingly, KO of either subunit also led to steady-state upregulation of the IFN-stimulated gene MX1, suggesting that defects in the HOPS complex drive spontaneous activation of type I IFN (Figure 4D).

Overall, we show that the HOPS complex subunits VPS11 and VPS33A regulate STING degradation. Blocking STING degradation results in increased phosphorylation of STING with consequent higher transcription of downstream IFN-β and IL-6 and upregulation of MX1 at steady state.

RIC1 and VPS52 regulate STING trafficking at the Golgi

We then characterized genes from two other complexes that increased per-cell STING maximum intensity and were identified by SVM classifiers and unsupervised clustering to affect STING trafficking (Figures 2A and S4B). Specifically, we focused on the RAB6 GEF complex composed of RIC1 and RGP1 and the RAB6-interacting GARP complex.[54,55] Mutations in either RIC1 or subunits of the GARP complex have been associated with neurodegenerative disease in the human population. The KO mouse for the GARP subunit VPS54, known as the Wobbler mouse, is a model of ALS.[56–58] In the genome-wide screen, RIC1 and RGP1 clustered together in cluster 0 and subunits of the GARP complex (VPS51, VPS52, VPS53, and VPS54) clustered in cluster 67 with GET4, a protein involved in Golgi-to-ER trafficking and protein quality control[59] and PITPNB, which is required for coat protein complex I (COPI)-mediated retrograde transport from the Golgi[60] (Figure 5A). RIC1 was found enriched at 0.5 and 1 h in the proximity of STING[8] (Figure S5A) and is part of the RIC1-RGP1 complex that regulates guanosine diphosphate (GDP)-GTP exchange on RAB6, a RAB protein involved in the secretory pathway.[61,62] The VPS52 subunit of the GARP

complex, a complex involved in endosome-to-Golgi recycling and membrane fusion at the Golgi, interacts with GTP-bound RAB6.[63] Additionally, the constitutively active STING V155M found in SAVI patients has been shown to colocalize with RAB6 at steady state.[64] We therefore hypothesized that both RIC1 and VPS52 regulate STING trafficking between the Golgi and the endosome.

We knocked out RIC1 or VPS52 in our STING-mNG reporter line (Figures S5B–S5D). KO of either protein with two independent guides per gene led to a reduction in STING degradation (Figures 5B and 5C), suggesting that both complexes play a role in STING trafficking. KO of either gene in BJ1 fibroblasts also led to a reduction in STING degradation upon stimulation, consistent with the reporter line, and led to an increase in pSTING, pTBK1, and pIRF3 downstream signaling while not affecting LC3B lipidation (Figures 5D and 5E). These results suggest that RIC1 and VPS52 regulate STING signaling shutdown in addition to STING degradation, while they do not affect STING-dependent activation of autophagy or autophagy resolution. In order to validate the impact of each gene KO on STING trafficking at the Golgi, as predicted from our screens, we performed immunofluorescence in BJ1 fibroblasts that were either KO for RIC1 or VPS52. KO of each gene led to STING accumulation in the Golgi, shown by increased colocalization of STING and GM130 upon stimulation (Figures 5F–5I). Increased colocalization of STING and GM130 was particularly evident in RIC1 KO cells at 1 h, and either RIC1 or VPS52 KO led to an increase in colocalization at the 3 h time point, suggesting that both genes regulate STING exit from the Golgi. Increased Golgi dwell time in KO cells is consistent with an increase in pSTING levels due to a delay in STING trafficking and degradation (Figures 5D and 5E).

Overall, these data show that the RIC1-RGP1 complex and the VPS52 subunit of the GARP complex regulate STING trafficking and Golgi exit.

DISCUSSION

STING trafficking is central to innate responses driven by dsDNA of exogenous or endogenous origin. While activation of this pathway is essential to achieve effective antitumor responses, dysregulation of this process has been linked to disease. In order to identify genes regulating STING trafficking in an unbiased manner and facilitate the association of a genetic perturbation to a subcellular trafficking phenotype, we leveraged OPS. We carried

Figure 5. The RAB6 GEF RIC1 and the GARP complex subunit VPS52 regulate STING Golgi exit

(A) STRING network of interaction of the indicated proteins found in clusters 0 and 67 of the dimensionality reduced data shown in Figure 2C.

(B) mNG levels in 293 T STING-mNG cell lines KO for the indicated genes stimulated with 4 μg/mL 2'3'-cGAMP(pS)2 (in medium) for 6 h. One representative plot of *n* = 3 independent experiments with *n* = 2 technical replicates per experiment.

(C) Percentage of STING-mNG-positive cells in cells stimulated as in (B).

(D) Immunoblot of the indicated proteins in BJ1 fibroblasts transduced with a control guide (ntgRNA) or with RIC1 sgRNAs and stimulated with 1 μM diABZI for the indicated times.

(E) Same as in (D) for VPS52 KO cells.

(F) Immunofluorescence of DAPI (blue), GM130 (magenta), and STING (yellow) in control (ntgRNA) or RIC1 KO BJ1 fibroblasts stimulated with 1 μM diABZI for the indicated times. One field representative of *n* ≥ 3 in *n* = 3 independent experiments.

(G) STING mean intensity calculated in GM130 (Golgi) regions in cells as in (F). Each dot represents an individual Golgi.

(H) Same as in (E) for VPS52 KO cells.

(I) STING mean intensity calculated in GM130 (Golgi) regions in cells as in (H). Each dot represents an individual Golgi.

In all panels, bar plots show mean and error bars standard deviation. Marker unit for western blots is kDa. *p <0.05,**p <0.01, ***p <0.001,****p < 0.0001; ns, not significant.

out one of the largest reported genome-wide OPS (over 45 million single-cell images assigned to genetic perturbations) and imaged cellular markers in 5 channels. We used SVM classifiers to identify genes with statistically significant effects on STING trafficking and guide data interpretation and showed that this high-dimensional dataset performed better than previously performed CRISPR screens with flow cytometric or fitness readouts. Clustering of our high-content imaging dataset guided gene functional assignment. For example, we show that the recently characterized autophagy gene EI24[41] plays a role in STING degradation and signaling shutdown based on its clustering neighbor ATG9A, which was previously known to regulate STING trafficking.[42]

To further confirm gene function assignment to phenotype, we performed targeted secondary OPS. To increase the information content of the screen, we integrated the iterative 4i staining protocol in the OPS pipeline, allowing us to image a total of 11 cellular markers. Additionally, we also performed for the first time an OPS in hTERT-immortalized primary cells, specifically BJ1 fibroblasts. Based on these datasets, we performed further clustering, which allowed us to assign a function to the poorly characterized gene C19orf25. C19orf25 clustered with USE1, a known regulator of Golgi-to-ER retrograde transport, and we show that KO of C19orf25 phenotypically mimics USE1 KO on STING trafficking, potentially through blocking STING Golgi-to-ER recycling.

By focusing on protein complexes that have mutations in the human population associated with disease but have not been shown to regulate STING trafficking, we also identified new roles for the HOPS, GARP, and RIC1-RGP1 complexes in STING biology. We show that KO of the HOPS complex blocks STING degradation, similar to VPS37A KO that clustered with HOPS complex perturbations, and that we previously demonstrated to regulate STING trafficking.[8] Similar to ESCRT KO or dysfunction, VPS11 and VPS33A KO lead to steady-state upregulation of the ISG MX1, suggesting that defects in the HOPS complex activate spontaneous type I IFN responses. STING vesicles are LC3B-lipidated post-Golgi via CASM.[46,47] The HOPS complex has an established role in driving fusion of autophagosomes with RAB7$^+$ endolysosomes.[50] We speculate that the HOPS complex could help in fusion of STING-containing LC3B-lipidated vesicles with the endolysosome to achieve STING signaling shutdown. Under this hypothesis, defects in the complex would result in increased STING signaling. Interestingly, mutations in both VPS11 and VPS33A have been found in patients with neurodegenerative disease.[51,52] Exacerbated activation of STING via dysregulation of its trafficking has been associated with neurodegeneration in multiple diseases such as Niemann-Pick disease and ALS.[21,22,65] The impact of HOPS complex KO on STING signaling raises the possibility that dysfunction of this complex leads to exacerbated STING activation and subsequent pathogenesis in patients.

We also show that the RAB6 GEF complex composed of RIC1-RGP1 and the GARP complex subunit VPS52, which interacts with GTP-loaded RAB6, regulates STING exit from the Golgi. KO of either gene leads to a delay in Golgi exit of STING upon stimulation, resulting in increased phosphorylation of STING and downstream TBK1 and IRF3. The GARP complex regulates endosome-to-Golgi recycling by promoting fusion of vesicles originating from the recycling endosome with the Golgi.[63] STING has been shown to traffic to the recycling endosome, and STING-containing vesicles originating from this compart-

ment are then degraded in an ESCRT-dependent manner.[8–10] Interestingly, in our proximity-ligation proteomics dataset, GO analysis showed enrichment of "retrograde transport at the *trans*-Golgi-network" at 2 h post STING stimulation.[8] Involvement of the GARP complex in STING trafficking opens the possibility that an endosome-to-Golgi recycling pathway could be present to recycle activated STING, analogous to Golgi-to-ER STING retrograde trafficking.[16–18,20]

Overall, we present here a collection of pooled screening results, including a powerful, high-content genome-wide OPS that constitutes a broad data resource for the immunology community. Integration with other results and further analysis may aid the identification of additional genes and mechanisms regulating STING trafficking and function. This data resource will also be of value to identify points of intervention in STING's involvement in disease resulting from dysregulation of its trafficking or to boost STING responses in the context of antitumor immunity.

RESOURCE AVAILABILITY

Lead contact
Requests for further information and resources should be directed to and will be fulfilled by the lead contact, Nir Hacohen (nhacohen@broadinstitute.org).

Materials availability
Plasmids generated in this study have been deposited at Addgene (#227185, #227186).

Data and code availability
- Processed flow cytometry and optical pooled screening data are publicly available as supplemental information or at Zenodo as of the date of publication. DOIs are listed in the key resources table.
- Raw imaging data for the optical pooled screens are accessible via the gcloud CLI on Google Cloud Storage at gs://opspublic-east1/STIN-GOpticalPooledScreen.
- This paper analyzes existing, publicly available data. Accession numbers for the datasets are listed in the key resources table.
- All original code has been deposited at GitHub and Zenodo and is publicly available as of the date of publication. DOIs are listed in the key resources table.
- Any additional information required to reanalyze the data reported in this paper is available from the lead contact upon request.

Cell Systems
Article

STAR★METHODS

Detailed methods are provided in the online version of this paper and include the following:

- KEY RESOURCES TABLE
- METHOD DETAILS
  - Cell lines
  - Constructs
  - Viral transductions for cell line generation
  - Flow cytometry of 293T STING-mNG
  - RT-qPCR
  - Western blot
  - Immunofluorescence for follow-up studies
  - Image quantification for VPS52 and RIC1 Arrayed Knockout Experiments
  - OPS Library cloning, lentivirus production, transduction, and next generation sequencing of libraries
  - STING stimulation, phenotyping, and in situ sequencing for genome-wide optical pooled screen
  - Secondary optical pooled screens
  - Fluorescence microscopy
  - Phosphorylated STING flow cytometry screen
- QUANTIFICATION AND STATISTICAL ANALYSIS
  - Image analysis
  - Optical pooled screen analysis
  - Meta-Analysis by Information Content
  - Dimensionality reduction and clustering
  - Phosphorylated STING flow cytometry analysis

SUPPLEMENTAL INFORMATION

Supplemental information can be found online at https://doi.org/10.1016/j.cels.2024.11.004.

REFERENCES

1. Motwani, M., Pesiridis, S., and Fitzgerald, K.A. (2019). DNA sensing by the cGAS-STING pathway in health and disease. Nat. Rev. Genet. 20, 657–674. https://doi.org/10.1038/s41576-019-0151-1.

2. Samson, N., and Ablasser, A. (2022). The cGAS-STING pathway and cancer. Nat. Cancer 3, 1452–1463. https://doi.org/10.1038/s43018-022-00468-w.

3. Skopelja-Gardner, S., An, J., and Elkon, K.B. (2022). Role of the cGAS-STING pathway in systemic and organ-specific diseases. Nat. Rev. Nephrol. 18, 558–572. https://doi.org/10.1038/s41581-022-00589-6.

4. Yang, K., Tang, Z., Xing, C., and Yan, N. (2024). STING signaling in the brain: Molecular threats, signaling activities, and therapeutic challenges. Neuron 112, 539–557. https://doi.org/10.1016/j.neuron.2023.10.014.

5. Ishikawa, H., and Barber, G.N. (2008). STING is an endoplasmic reticulum adaptor that facilitates innate immune signalling. Nature 455, 674–678. https://doi.org/10.1038/nature07317.

6. Haag, S.M., Gulen, M.F., Reymond, L., Gibelin, A., Abrami, L., Decout, A., Heymann, M., van der Goot, F.G., Turcatti, G., Behrendt, R., et al. (2018). Targeting STING with covalent small-molecule inhibitors. Nature 559, 269–273. https://doi.org/10.1038/s41586-018-0287-8.

7. Mukai, K., Konno, H., Akiba, T., Uemura, T., Waguri, S., Kobayashi, T., Barber, G.N., Arai, H., and Taguchi, T. (2016). Activation of STING requires palmitoylation at the Golgi. Nat. Commun. 7, 11932. https://doi.org/10.1038/ncomms11932.

8. Gentili, M., Liu, B., Papanastasiou, M., Dele-Oni, D., Schwartz, M.A., Carlson, R.J., Al'Khafaji, A.M., Krug, K., Brown, A., Doench, J.G., et al. (2023). ESCRT-dependent STING degradation inhibits steady-state and cGAMP-induced signalling. Nat. Commun. 14, 611. https://doi.org/10.1038/s41467-023-36132-9.

9. Kuchitsu, Y., Mukai, K., Uematsu, R., Takaada, Y., Shinojima, A., Shindo, R., Shoji, T., Hamano, S., Ogawa, E., Sato, R., et al. (2023). STING signalling is terminated through ESCRT-dependent microautophagy of vesicles originating from recycling endosomes. Nat. Cell Biol. 25, 453–466. https://doi.org/10.1038/s41556-023-01098-9.

10. Balka, K.R., Venkatraman, R., Saunders, T.L., Shoppee, A., Pang, E.S., Magill, Z., Homman-Ludiye, J., Huang, C., Lane, R.M., York, H.M., et al. (2023). Termination of STING responses is mediated via ESCRT-dependent degradation. EMBO J. 42, e112712. https://doi.org/10.15252/embj.2022112712.

11. Gui, X., Yang, H., Li, T., Tan, X., Shi, P., Li, M., Du, F., and Chen, Z.J. (2019). Autophagy induction via STING trafficking is a primordial function of the cGAS pathway. Nature 567, 262–266. https://doi.org/10.1038/s41586-019-1006-9.

12. Liu, B., Carlson, R.J., Pires, I.S., Gentili, M., Feng, E., Hellier, Q., Schwartz, M.A., Blainey, P.C., Irvine, D.J., and Hacohen, N. (2023). Human STING is a proton channel. Science 381, 508–514. https://doi.org/10.1126/science.adf8974.

13. Xun, J., Zhang, Z., Lv, B., Lu, D., Yang, H., Shang, G., and Tan, J.X. (2024). A conserved ion channel function of STING mediates noncanonical autophagy and cell death. EMBO Rep 25, 544–569. https://doi.org/10.1038/s44319-023-00045-x.

14. Balka, K.R., Louis, C., Saunders, T.L., Smith, A.M., Calleja, D.J., D'Silva, D.B., Moghaddas, F., Tailler, M., Lawlor, K.E., Zhan, Y., et al. (2020). TBK1 and IKKε Act Redundantly to Mediate STING-Induced NF-κB Responses in Myeloid Cells. Cell Rep. 31, 107492. https://doi.org/10.1016/j.celrep.2020.03.056.

15. Tu, X., Chu, T.-T., Jeltema, D., Abbott, K., Yang, K., Xing, C., Han, J., Dobbs, N., and Yan, N. (2022). Interruption of post-Golgi STING trafficking activates tonic interferon signaling. Nat. Commun. 13, 6977. https://doi.org/10.1038/s41467-022-33765-0.

16. Steiner, A., Hrovat-Schaale, K., Prigione, I., Yu, C.-H., Laohamonthonkul, P., Harapas, C.R., Low, R.R.J., De Nardo, D., Dagley, L.F., Mlodzianoski, M.J., et al. (2022). Deficiency in coatomer complex I causes aberrant activation of STING signalling. Nat. Commun. 13, 2321. https://doi.org/10.1038/s41467-022-29946-6.

17. Deng, Z., Chong, Z., Law, C.S., Mukai, K., Ho, F.O., Martinu, T., Backes, B.J., Eckalbar, W.L., Taguchi, T., and Shum, A.K. (2020). A defect in COPI-mediated transport of STING causes immune dysregulation in COPA syndrome. J. Exp. Med. 217, e20201045. https://doi.org/10.1084/jem.20201045.

18. Mukai, K., Ogawa, E., Uematsu, R., Kuchitsu, Y., Kiku, F., Uemura, T., Waguri, S., Suzuki, T., Dohmae, N., Arai, H., et al. (2021). Homeostatic

regulation of STING by retrograde membrane traffic to the ER. Nat. Commun. *12*, 61. https://doi.org/10.1038/s41467-020-20234-9.

19. Watkin, L.B., Jessen, B., Wiszniewski, W., Vece, T.J., Jan, M., Sha, Y., Thamsen, M., Santos-Cortez, R.L.P., Lee, K., Gambin, T., et al. (2015). COPA mutations impair ER-Golgi transport and cause hereditary autoimmune-mediated lung disease and arthritis. Nat. Genet. *47*, 654–660. https://doi.org/10.1038/ng.3279.

20. Lepelley, A., Martin-Niclós, M.J., Le Bihan, M., Marsh, J.A., Uggenti, C., Rice, G.I., Bondet, V., Duffy, D., Hertzog, J., Rehwinkel, J., et al. (2020). Mutations in COPA lead to abnormal trafficking of STING to the Golgi and interferon signaling. J. Exp. Med. *217*, e20200600. https://doi.org/10.1084/jem.20200600.

21. McCauley, M.E., O'Rourke, J.G., Yáñez, A., Markman, J.L., Ho, R., Wang, X., Chen, S., Lall, D., Jin, M., Muhammad, A.K.M.G., et al. (2020). C9orf72 in myeloid cells suppresses STING-induced inflammation. Nature *585*, 96–101. https://doi.org/10.1038/s41586-020-2625-x.

22. Chu, T.-T., Tu, X., Yang, K., Wu, J., Repa, J.J., and Yan, N. (2021). Tonic prime-boost of STING signalling mediates Niemann-Pick disease type C. Nature *596*, 570–575. https://doi.org/10.1038/s41586-021-03762-2.

23. Gonugunta, V.K., Sakai, T., Pokatayev, V., Yang, K., Wu, J., Dobbs, N., and Yan, N. (2017). Trafficking-Mediated STING Degradation Requires Sorting to Acidified Endolysosomes and Can Be Targeted to Enhance Anti-tumor Response. Cell Rep. *21*, 3234–3242. https://doi.org/10.1016/j.celrep.2017.11.061.

24. Feldman, D., Singh, A., Schmid-Burgk, J.L., Carlson, R.J., Mezger, A., Garrity, A.J., Zhang, F., and Blainey, P.C. (2019). Optical Pooled Screens in Human Cells. Cell *179*, 787–799.e17. https://doi.org/10.1016/j.cell.2019.09.016.

25. Carlson, R.J., Leiken, M.D., Guna, A., Hacohen, N., and Blainey, P.C. (2023). A genome-wide optical pooled screen reveals regulators of cellular antiviral responses. Proc. Natl. Acad. Sci. USA *120*, e2210623120. https://doi.org/10.1073/pnas.2210623120.

26. Funk, L., Su, K.-C., Ly, J., Feldman, D., Singh, A., Moodie, B., Blainey, P.C., and Cheeseman, I.M. (2022). The phenotypic landscape of essential human genes. Cell *185*, 4634–4653.e22. https://doi.org/10.1016/j.cell.2022.10.017.

27. Li, B., Clohisey, S.M., Chia, B.S., Wang, B., Cui, A., Eisenhaure, T., Schweitzer, L.D., Hoover, P., Parkinson, N.J., Nachshon, A., et al. (2020). Genome-wide CRISPR screen identifies host dependency factors for influenza A virus infection. Nat. Commun. *11*, 164. https://doi.org/10.1038/s41467-019-13965-x.

28. Heigwer, F., Scheeder, C., Bageritz, J., Yousefian, S., Rauscher, B., Laufer, C., Beneyto-Calabuig, S., Funk, M.C., Peters, V., Boulougouri, M., et al. (2023). A global genetic interaction network by single-cell imaging and machine learning. Cell Syst. *14*, 346–362.e6. https://doi.org/10.1016/j.cels.2023.03.003.

29. McKinley, K.L., and Cheeseman, I.M. (2017). Large-Scale Analysis of CRISPR/Cas9 Cell-Cycle Knockouts Reveals the Diversity of p53-Dependent Responses to Cell-Cycle Defects. Dev. Cell *40*, 405–420.e2. https://doi.org/10.1016/j.devcel.2017.01.012.

30. Prabakaran, T., Bodda, C., Krapp, C., Zhang, B.-C., Christensen, M.H., Sun, C., Reinert, L., Cai, Y., Jensen, S.B., Skouboe, M.K., et al. (2018). Attenuation of cGAS-STING signaling is mediated by a p62/SQSTM1-dependent autophagy pathway activated by TBK1. EMBO J. *37*, e97858. https://doi.org/10.15252/embj.201797858.

31. McQuin, C., Goodman, A., Chernyshev, V., Kamentsky, L., Cimini, B.A., Karhohs, K.W., Doan, M., Ding, L., Rafelski, S.M., Thirstrup, D., et al. (2018). CellProfiler 3.0: Next-generation image processing for biology. PLoS Biol. *16*, e2005970. https://doi.org/10.1371/journal.pbio.2005970.

32. van der Walt, S., Schönberger, J.L., Nunez-Iglesias, J., Boulogne, F., Warner, J.D., Yager, N., Gouillart, E., and Yu, T.; scikit-image contributors (2014). scikit-image: image processing in Python. PeerJ *2*, e453. https://doi.org/10.7717/peerj.453.

33. Coelho, L.P. (2012). Mahotas: Open source software for scriptable computer vision. Preprint at arXiv.

34. Moon, K.R., van Dijk, D., Wang, Z., Gigante, S., Burkhardt, D.B., Chen, W.S., Yim, K., van den Elzen, A.V.D., Hirn, M.J., Coifman, R.R., et al. (2019). Visualizing structure and transitions in high-dimensional biological data. Nat. Biotechnol. *37*, 1482–1492. https://doi.org/10.1038/s41587-019-0336-3.

35. Traag, V., Waltman, L., and van Eck, N.J. (2018). From Louvain to Leiden: guaranteeing well-connected communities. Sci. Rep. *9*, 5233.

36. Chen, W., Li, S., Yu, H., Liu, X., Huang, L., Wang, Q., Liu, H., Cui, Y., Tang, Y., Zhang, P., et al. (2016). ER Adaptor SCAP Translocates and Recruits IRF3 to Perinuclear Microsome Induced by Cytosolic Microbial DNAs. PLoS Pathog. *12*, e1005462. https://doi.org/10.1371/journal.ppat.1005462.

37. Fei, X., Huang, J., Li, F., Wang, Y., Shao, Z., Dong, L., Wu, Y., Li, B., Zhang, X., Lv, B., et al. (2023). The Scap-SREBP1-S1P/S2P lipogenesis signal orchestrates the homeostasis and spatiotemporal activation of NF-κB. Cell Rep. *42*, 112586. https://doi.org/10.1016/j.celrep.2023.112586.

38. Watson, P., Forster, R., Palmer, K.J., Pepperkok, R., and Stephens, D.J. (2005). Coupling of ER exit to microtubules through direct interaction of COPII with dynactin. Nat. Cell Biol. *7*, 48–55. https://doi.org/10.1038/ncb1206.

39. Replogle, J.M., Saunders, R.A., Pogson, A.N., Hussmann, J.A., Lenail, A., Guna, A., Mascibroda, L., Wagner, E.J., Adelman, K., Lithwick-Yanai, G., et al. (2022). Mapping information-rich genotype-phenotype landscapes with genome-scale Perturb-seq. Cell *185*, 2559–2575.e28. https://doi.org/10.1016/j.cell.2022.05.013.

40. Giurgiu, M., Reinhard, J., Brauner, B., Dunger-Kaltenbach, I., Fobo, G., Frishman, G., Montrone, C., and Ruepp, A. (2019). CORUM: the comprehensive resource of mammalian protein complexes—2019. Nucleic Acids Res. *47*, D559–D563. https://doi.org/10.1093/nar/gky973.

41. Zheng, Q., Chen, Y., Chen, D., Zhao, H., Feng, Y., Meng, Q., Zhao, Y., and Zhang, H. (2022). Calcium transients on the ER surface trigger liquid-liquid phase separation of FIP200 to specify autophagosome initiation sites. Cell *185*, 4082–4098.e22. https://doi.org/10.1016/j.cell.2022.09.001.

42. Saitoh, T., Fujita, N., Hayashi, T., Takahara, K., Satoh, T., Lee, H., Matsunaga, K., Kageyama, S., Omori, H., Noda, T., et al. (2009). Atg9a controls dsDNA-driven dynamic translocation of STING and the innate immune response. Proc. Natl. Acad. Sci. USA *106*, 20842–20846. https://doi.org/10.1073/pnas.0911267106.

43. Gut, G., Herrmann, M.D., and Pelkmans, L. (2018). Multiplexed protein maps link subcellular organization to cellular states. Science *361*. https://doi.org/10.1126/science.aar7042.

44. Sternberg. (1983). Biomedical Image Processing. Computer *16*, 22–34. https://doi.org/10.1109/MC.1983.1654163.

45. Wainberg, M., Kamber, R.A., Balsubramani, A., Meyers, R.M., Sinnott-Armstrong, N., Hornburg, D., Jiang, L., Chan, J., Jian, R., Gu, M., et al. (2021). A genome-wide atlas of co-essential modules assigns function to uncharacterized genes. Nat. Genet. *53*, 638–649. https://doi.org/10.1038/s41588-021-00840-z.

46. Fischer, T.D., Wang, C., Padman, B.S., Lazarou, M., and Youle, R.J. (2020). STING induces LC3B lipidation onto single-membrane vesicles via the V-ATPase and ATG16L1-WD40 domain. J. Cell Biol. *219*, e202009128. https://doi.org/10.1083/jcb.202009128.

47. Hooper, K.M., Jacquin, E., Li, T., Goodwin, J.M., Brumell, J.H., Durgan, J., and Florey, O. (2022). V-ATPase is a universal regulator of LC3-associated phagocytosis and non-canonical autophagy. J. Cell Biol. *221*, e202105112. https://doi.org/10.1083/jcb.202105112.

48. Dilcher, M., Veith, B., Chidambaram, S., Hartmann, E., Schmitt, H.D., and Fischer von Mollard, G. (2003). Use1p is a yeast SNARE protein required for retrograde traffic to the ER. EMBO J. *22*, 3664–3674. https://doi.org/10.1093/emboj/cdg339.

49. Szklarczyk, D., Gable, A.L., Lyon, D., Junge, A., Wyder, S., Huerta-Cepas, J., Simonovic, M., Doncheva, N.T., Morris, J.H., Bork, P., et al. (2019). STRING v11: protein–protein association networks with increased coverage, supporting functional discovery in genome-wide experimental

datasets. Nucleic Acids Res. *47*, D607–D613. https://doi.org/10.1093/nar/gky1131.

50. Shvarev, D., Schoppe, J., König, C., Perz, A., Füllbrunn, N., Kiontke, S., Langemeyer, L., Januliene, D., Schnelle, K., Kümmel, D., et al. (2022). Structure of the HOPS tethering complex, a lysosomal membrane fusion machinery. eLife *11*, e80901. https://doi.org/10.7554/eLife.80901.

51. Zhang, J., Lachance, V., Schaffner, A., Li, X., Fedick, A., Kaye, L.E., Liao, J., Rosenfeld, J., Yachelevich, N., Chu, M.-L., et al. (2016). A Founder Mutation in VPS11 Causes an Autosomal Recessive Leukoencephalopathy Linked to Autophagic Defects. PLoS Genet. *12*, e1005848. https://doi.org/10.1371/journal.pgen.1005848.

52. Pavlova, E.V., Shatunov, A., Wartosch, L., Moskvina, A.I., Nikolaeva, L.E., Bright, N.A., Tylee, K.L., Church, H.J., Ballabio, A., Luzio, J.P., et al. (2019). The lysosomal disease caused by mutant VPS33A. Hum. Mol. Genet. *28*, 2514–2530. https://doi.org/10.1093/hmg/ddz077.

53. Balderhaar, H.J.K., and Ungermann, C. (2013). CORVET and HOPS tethering complexes – coordinators of endosome and lysosome fusion. J. Cell Sci. *126*, 1307–1316. https://doi.org/10.1242/jcs.107805.

54. Homma, Y., and Fukuda, M. (2021). Knockout analysis of Rab6 effector proteins revealed the role of VPS52 in the secretory pathway. Biochem. Biophys. Res. Commun. *561*, 151–157. https://doi.org/10.1016/j.bbrc.2021.05.009.

55. Pusapati, G.V., Luchetti, G., and Pfeffer, S.R. (2012). Ric1-Rgp1 complex is a guanine nucleotide exchange factor for the late Golgi Rab6A GTPase and an effector of the medial Golgi Rab33B GTPase. J. Biol. Chem. *287*, 42129–42137. https://doi.org/10.1074/jbc.M112.414565.

56. Unlu, G., Qi, X., Gamazon, E.R., Melville, D.B., Patel, N., Rushing, A.R., Hashem, M., Al-Faifi, A., Chen, R., Li, B., et al. (2020). Phenome-based approach identifies RIC1-linked Mendelian syndrome through zebrafish models, biobank associations and clinical studies. Nat. Med. *26*, 98–109. https://doi.org/10.1038/s41591-019-0705-y.

57. Feinstein, M., Flusser, H., Lerman-Sagie, T., Ben-Zeev, B., Lev, D., Agamy, O., Cohen, I., Kadir, R., Sivan, S., Leshinsky-Silver, E., et al. (2014). VPS53 mutations cause progressive cerebello-cerebral atrophy type 2 (PCCA2). J. Med. Genet. *51*, 303–308. https://doi.org/10.1136/jmedgenet-2013-101823.

58. Schmitt-John, T. (2015). VPS54 and the wobbler mouse. Front. Neurosci. *9*, 381. https://doi.org/10.3389/fnins.2015.00381.

59. Tambe, M.A., Ng, B.G., Shimada, S., Wolfe, L.A., Adams, D.R., Undiagnosed Diseases Network, Gahl, W.A., Bamshad, M.J., Nickerson, D.A., Malicdan, M.C.V., et al. (2020). Mutations in GET4 disrupt the transmembrane domain recognition complex pathway. J. Inherit. Metab. Dis. *43*, 1037–1045. https://doi.org/10.1002/jimd.12249.

60. Carvou, N., Holic, R., Li, M., Futter, C., Skippen, A., and Cockcroft, S. (2010). Phosphatidylinositol- and phosphatidylcholine-transfer activity of PITPbeta is essential for COPI-mediated retrograde transport from the Golgi to the endoplasmic reticulum. J. Cell Sci. *123*, 1262–1273. https://doi.org/10.1242/jcs.061986.

61. Grigoriev, I., Splinter, D., Keijzer, N., Wulf, P.S., Demmers, J., Ohtsuka, T., Modesti, M., Maly, I.V., Grosveld, F., Hoogenraad, C.C., et al. (2007). Rab6 regulates transport and targeting of exocytotic carriers. Dev. Cell *13*, 305–314. https://doi.org/10.1016/j.devcel.2007.06.010.

62. Patwardhan, A., Bardin, S., Miserey-Lenkei, S., Larue, L., Goud, B., Raposo, G., and Delevoye, C. (2017). Routing of the RAB6 secretory pathway towards the lysosome related organelle of melanocytes. Nat. Commun. *8*, 15835. https://doi.org/10.1038/ncomms15835.

63. Khakurel, A., and Lupashin, V.V. (2023). Role of GARP Vesicle Tethering Complex in Golgi Physiology. Int. J. Mol. Sci. *24*, 6069. https://doi.org/10.3390/ijms24076069.

64. Jeremiah, N., Neven, B., Gentili, M., Callebaut, I., Maschalidi, S., Stolzenberg, M.C., Goudin, N., Frémond, M.L., Nitschke, P., Molina, T.J., et al. (2014). Inherited STING-activating mutation underlies a familial inflammatory syndrome with lupus-like manifestations. J. Clin. Invest. *124*, 5516–5520. https://doi.org/10.1172/JCI79100.

65. Yu, C.-H., Davidson, S., Harapas, C.R., Hilton, J.B., Mlodzianoski, M.J., Laohamonthonkul, P., Louis, C., Low, R.R.J., Moecking, J., De Nardo, D., et al. (2020). TDP-43 Triggers Mitochondrial DNA Release via mPTP to Activate cGAS/STING in ALS. Cell *183*, 636–649.e18. https://doi.org/10.1016/j.cell.2020.09.020.

66. Spitzer, H., Berry, S., Donoghoe, M., Pelkmans, L., and Theis, F.J. (2023). Learning consistent subcellular landmarks to quantify changes in multiplexed protein maps. Nat. Methods *20*, 1058–1069. https://doi.org/10.1038/s41592-023-01894-z.

67. Feldman, D., Funk, L., Le, A., Carlson, R.J., Leiken, M.D., Tsai, F., Soong, B., Singh, A., and Blainey, P.C. (2022). Pooled genetic perturbation screens with image-based phenotypes. Nat. Protoc. *17*, 476–512. https://doi.org/10.1038/s41596-021-00653-8.

68. Köster, J., and Rahmann, S. (2012). Snakemake–a scalable bioinformatics workflow engine. Bioinformatics *28*, 2520–2522. https://doi.org/10.1093/bioinformatics/bts480.

69. Bray, M.-A., Singh, S., Han, H., Davis, C.T., Borgeson, B., Hartland, C., Kost-Alimova, M., Gustafsdottir, S.M., Gibson, C.C., and Carpenter, A.E. (2016). Cell Painting, a high-content image-based assay for morphological profiling using multiplexed fluorescent dyes. Nat. Protoc. *11*, 1757–1774. https://doi.org/10.1038/nprot.2016.105.

70. Pedregosa, F., Varoquaux, G., Gramfort, A., Michel, V., Thirion, B., Grisel, O., Blondel, M., Prettenhofer, P., Weiss, R., Dubourg, V., et al. (2011). Scikit-learn: Machine Learning in Python. J. Mach. Learn. Res. *12*, 2825–2830.

71. Hubert, L., and Arabie, P. (1985). Comparing partitions. J. Classif. *2*, 193–218. https://doi.org/10.1007/BF01908075.

72. Wolf, F.A., Angerer, P., and Theis, F.J. (2018). SCANPY: large-scale single-cell gene expression data analysis. Genome Biol. *19*, 15. https://doi.org/10.1186/s13059-017-1382-0.

STAR★METHODS

KEY RESOURCES TABLE

REAGENT or RESOURCE	SOURCE	IDENTIFIER
Antibodies		
p65	Cell Signaling Technology	Cat# 6956; RRID:AB_10828935
GM130	Cell Signaling Technology	Cat# 12480; RRID:AB_2797933
Actin	Cell Signaling Technology	Cat# 3700; RRID:AB_2242334
HGS	Cell Signaling Technology	Cat# 15087; RRID:AB_2798700
gH2AX	Millipore	Cat# 05-636; RRID:AB_309864
Calnexin	Abcam	Cat# ab22595; RRID:AB_2069006
EEA1	BD Biosciences	Cat# 610456; RRID:AB_397829
ATP6V1D	Abcam	Cat# ab157458; RRID:AB_2732041
Anti-mouse AF555+	Thermo Fisher	Cat# A32773; RRID:AB_2762848
Anti-rabbit AF647+	Thermo Fisher	Cat# A32795; RRID:AB_2762835
HRP Anti-beta Actin antibody [AC-15]	Abcam	Cat# ab49900; RRID:AB_867494
STING (D2P2F)	Cell Signaling Technology	Cat# 13647; RRID:AB_2732796
pSTING (Ser366) (D7C3S)	Cell Signaling Technology	Cat# 19781; RRID:AB_2737062
TBK1 (E8I3G)	Cell Signaling Technology	Cat# 38066; RRID:AB_2827657
TBK1 (E9H5S)	Cell Signaling Technology	Cat# 51872; RRID:AB_2799403
pTBK1 (Ser172) (D52C2)	Cell Signaling Technology	Cat# 5483; RRID:AB_10693472
IRF3 (D6I4C)	Cell Signaling Technology	Cat# 11904; RRID:AB_2722521
pIRF3 (Ser386) (E7J8G)	Cell Signaling Technology	Cat# 37829; RRID:AB_2799121
MX1 (D3W7I)	Cell Signaling Technology	Cat# 37849; RRID:AB_2799122
LC3B	Cell Signaling Technology	Cat# 2775; RRID:AB_915950
DYKDDDDK Tag (D6W5B) - FLAG	Cell Signaling Technology	Cat# 14793; RRID:AB_2572291
VPS52	Millipore	Cat# SAB2106153; RRID:AB_10743509
VPS33A	Proteintech	Cat# 16896-1-AP; RRID:AB_2214916
VPS11	Santa Cruz	Cat# sc-515094; RRID:AB_2687986
TGN38	BD Biosciences	Cat# 610898; RRID:AB_10015241
CD63 (EPR22458-280)	Abcam	Cat# ab252919
STING	BD Biosciences	Cat# 564835; RRID:AB_2738973
GM130 (35/GM130)	BD Biosciences	Cat# 610823; RRID:AB_398142
GM130 (35/GM130)	Biolegend	Cat# 937001; RRID:AB_2888895
p62 (D5L7G)	Cell Signaling Technology	Cat# 88588; RRID:AB_2800125
Alexa 488 anti-mouse IgG (H+L)	Thermo Fisher	Cat# A-11029; RRID:AB_2534088
Alexa 555 F(ab')2 anti- Rabbit IgG	Thermo Fisher	Cat# A-21430; RRID:AB_2535851
Alexa 647 anti-rat IgG (H+L)	Thermo Fisher	Cat# A-21247; RRID:AB_141778
BV421-conjugated anti-CD63 (genome-wide screen)	BioLegend	Cat#353029, RRID:AB_2687003
Critical commercial assays		
RevertAid H minus Reverse Transcriptase	Thermo Fisher Scientific	Cat#EP0452
Ribolock RNase inhibitor	Thermo Fisher Scientific	Cat#EO0384
RNase H	Enzymatics	Cat#Y9220L
TaqIT DNA polymerase	Enzymatics	Cat#P7620L
Ampligase	Lucigen	Cat#A3210K
Phi29 DNA polymerase	Thermo Fisher Scientific	Cat#EP0091
MiSeq Reagent Nano Kit v2 with PR2 buffer	Illumina	Cat#MS-103-1003
Deposited data		
Raw images	This paper	gs://opspublic-east1/ STINGOpticalPooledScreen (via glcoud CLI)

(Continued on next page)

Continued

REAGENT or RESOURCE	SOURCE	IDENTIFIER
Processed image features. HeLa Genome-wide Screen Single-Cell Features (Part 1/5)	This paper	https://zenodo.org/doi/10.5281/zenodo.12616517
Processed image features. STING OPS: HeLa Genome-wide Screen Single-Cell Features (Part 2/5)	This paper	https://zenodo.org/doi/10.5281/zenodo.12616551
Processed image features. STING OPS: HeLa Genome-wide Screen Single-Cell Features (Part 3/5)	This paper	https://zenodo.org/doi/10.5281/zenodo.12625005
Processed image features. STING OPS: HeLa Genome-wide Screen Single-Cell Features (Part 4/5)	This paper	https://zenodo.org/doi/10.5281/zenodo.12625007
Processed image features. STING OPS: HeLa Genome-wide Screen Single-Cell Features (Part 5/5)	This paper	https://zenodo.org/doi/10.5281/zenodo.12625247
Processed image features. STING OPS: HeLa Unstimulated Secondary Screen Single-Cell Features	This paper	https://zenodo.org/doi/10.5281/zenodo.12616016
Processed image features. STING OPS: HeLa Unstimulated Secondary Screen Single-Cell Features (Background-Subtracted)	This paper	https://zenodo.org/doi/10.5281/zenodo.12616198
Processed image features. STING OPS: HeLa cGAMP (4 hours) Secondary Screen Single-Cell Features	This paper	https://zenodo.org/doi/10.5281/zenodo.12616256
Processed image features. STING OPS: HeLa cGAMP (6 hours) Secondary Screen Single-Cell Features	This paper	https://zenodo.org/doi/10.5281/zenodo.12613850
Processed image features. STING OPS: BJ1 Secondary Screen Single-Cell Features	This paper	https://zenodo.org/doi/10.5281/zenodo.12613608
Genome-wide Perturb-seq data	https://doi.org/10.1016/j.cell.2022.05.013	SRA BioProject PRJNA83 https://doi.org/10.1038/s41596-021-00653-81566
Clinvar data	https://doi.org/10.1093/nar/gkx1153	https://ftp.ncbi.nlm.nih.gov/pub/clinvar/tab_delimited/archive/2022/gene_specific_summary_2022-05.txt.gz
Experimental models: Cell lines		
293T	ATCC	Cat# CRL-3216
BJ-5ta	ATCC	Cat# CRL-4001
U-937	ATCC	Cat# CRL-1593.2
HeLa-TetR-Cas9	Iain Cheeseman Lab, Whitehead Institute	N/A
Oligonucleotides		
sgRNA for screens and follow-up - see Table S9	This paper	N/A
IFNB1 FWD - CAGCATCTGCTGGTTGAAGA	This paper	N/A
IFNB1 RV - CATTACCTGAAGGCCAAGGA	This paper	N/A
IL6 FWD - CCCCTGACCCAACCACAAAT	This paper	N/A
IL6 RV - ATTTGCCGAAGAGCCCTCAG	This paper	N/A
GAPDH FWD - GTCTCCTCTGACTTCAACAGCG	This paper	N/A
GAPDH RV - ACCACCCTGTTGCTGTAGCCAA	This paper	N/A
oRT_CROPseq-v2 (for use with CROPseq-puro-v2): A+CT+CG+GT+GC+CA+CT+TTT	https://doi.org/10.1016/j.cell.2019.09.016	N/A
oPD_CROPseq-v2 (for use with CROPseq-puro- v2):/5Phos/GTTTCAGAGCTATGCTCTCCTGTTCGCCAAATTCTACCCACCACCCACTCTCCAaaggacgaaaCACCg	https://doi.org/10.1016/j.cell.2022.10.017	N/A
oSBS_CROPseq-v2 (for use with oPD_ CROPseq-v2): GCCAAATTCTACCCACCACCCACTCTCCAaaggacgaaaCACCg	https://doi.org/10.1016/j.cell.2022.10.017	N/A
oDF344 (Sg-guide amplification forward primer) ACACGACGCTCTTCCGATCTtcttgtggaaaggacgaaac	https://doi.org/10.1016/j.cell.2022.10.017	N/A

(Continued on next page)

Continued

REAGENT or RESOURCE	SOURCE	IDENTIFIER
oDF112 (Sg-guide amplification reverse primer) CTGGAGTTCAGACGTGTGCTCTTCCGATC aagcaccgactcggtgccac	https://doi.org/10.1016/j.cell.2022.10.017	N/A
Recombinant DNA		
CROPseq-puro-v2	Addgene	Cat# 127458
lentiCRISPR v2	GPP Broad Institute	Addgene cat# 52961
pTRIP-UbC-Blast-2A-STING-mNeonGreen	https://doi.org/10.1038/s41467-023-36132-9	N/A
pTRIP-hPGK-Blast-2A-STING-mNeonGreen	This manuscript	N/A
psPAX2	Addgene	Cat# 12260
pCMV-VSV-G	Addgene	Cat #8454
Software and algorithms		
Fiji	https://doi.org/10.1038/nmeth.2019	https://fiji.sc/
Graphpad Prism	Graphpad	https://www.graphpad.com/
FlowJo	BD Life Sciences	https://www.flowjo.com/
CellProfiler	https://doi.org/10.1186/s12859-021-04344-9	https://cellprofiler.org/
General repository used for processing optical pooled screening data	https://doi.org/10.1038/s41596-021-00653-8	https://github.com/feldman4/OpticalPooledScreens (https://zenodo.org/records/5002685)
Application-specific tools for the screens presented in this paper	This paper	https://github.com/beccajcarlson/STINGOpticalPooledScreen (https://zenodo.org/records/13761382)
Snakemake	https://doi.org/10.1093/bioinformatics/bty350	https://snakemake.readthedocs.io/en/stable/

METHOD DETAILS

Cell lines

HeLa cells were described previously[24] and had been transduced with a doxycycline-inducible Cas9 construct.[29] 293T were obtained from ATCC. 293T STING-mNeonGreen were described in Gentili et al.[8] BJ-5ta (hTERT immortalized primary BJ fibroblasts - referred to as BJ1 in the text) were obtained from ATCC. HeLa, HeLa-TetR-Cas9, and 293T were cultured in DMEM (Thermo Fisher) supplemented with 10% FBS (VWR), 1X Glutamax (Thermo Fisher) and 1% Penicillin/Streptomycin (Thermo Fisher). BJ-5ta were cultured in a 4:1 mix of DMEM (Thermo Fisher) and Medium 199 (Thermo Fisher) supplemented with 10% FBS (VWR), 1X Glutamax (Thermo Fisher) and 1% Penicillin/Streptomycin (Thermo Fisher). U937 were obtained from ATCC and cultured in RPMI (Gibco), 10% FBS (VWR), 1X Glutamax (Thermo Fisher) and 1% Penicillin/Streptomycin (Thermo Fisher). Cells were used up to passage 20 and were regularly tested for mycoplasma.

Constructs

Doxycycline-inducible Cas9 was described previously.[29] For optical pooled screens, sgRNAs were cloned into the CROPseq-puro-v2 backbone (Addgene #127458). pXPR_BRD023 (lentiCRISPR v2) was a kind gift of the Broad GPP platform. sgRNAs for follow-up KOs were ordered as ssDNA oligos from Azenta and cloned in BsmBI digested pXPR_BRD023 with T4 DNA ligase (NEB). All sgRNA sequences are listed in Table S9. pTRIP-UbC-Blast-2A-STING-mNeonGreen was expressed in 293T STING-mNG and was described in Gentili et al.[8] pTRIP-hPGK-Blast-2A-STING-mNeonGreen for expression in HeLa was obtained by substituting the UbC promoter for hPGK in pTRIP-UbC-Blast-2A-STING-mNeonGreen via PCR and Gibson assembly. psPAX2 (#12260) and pCMV-VSVG (#8454) were obtained from Addgene.

Viral transductions for cell line generation

0.8 million 293T were seeded on the day of transduction in one well of a tissue culture treated 6 well plate. Cells were transfected with a mix containing 200μl OptiMEM (Thermo Fisher), 8μl TransIT-293 (Mirus Bio), 1μg psPAX2, 0.4μg pCMV-VSV-G and 1.6μg of construct DNA. 8μl TransIT were incubated in 200μl OptiMEM for 1 hour at room temperature (RT). DNA was then added to the mix, and the mix was shaken and incubated at RT for 30 minutes. 208μl/well of mix was then added to 293T. Medium was changed to 3ml of fresh 293T medium after overnight incubation. Virus supernatant was harvested 30-34 hours after medium change and

filtered on 0.45μM syringe filters. 1 million 293T STING-mNG or 0.5 million BJ1 seeded the same day in one well of a 6 well plate were transduced with 2ml of virus including 8μg/ml Protamine (Thermo Fisher). Cells were incubated with viral supernatant for 1-2 days and cells were then transferred in a fresh flask for selection. Cells were then selected with the appropriate antibiotic: 2μg/ml Puromycin (Invivogen), 15μg/ml Blasticidin (Invivogen), 320μg/ml Hygromycin (Invivogen).

Flow cytometry of 293T STING-mNG
For flow cytometry analysis of 293T STING-mNG, 0.15 million cells were seeded in tissue culture treated 24w plates the day before stimulation. Cells were then stimulated with 4μg/ml of cGAMP(pS)2 (Invivogen) for 6 hours. Cells were then lifted with TrypLE (Thermo Fisher), washed in medium and resuspended in MACS buffer (0.5% BSA, 2mM EDTA). Acquisition was performed on a Cytoflex S or Cytoflex LX (Beckman Coulter). Data were analyzed with FlowJo (BD).

RT-qPCR
BJ1 fibroblasts were stimulated as described in figure legends. Cells were harvested and pellets were frozen at -80°C until processing. RNA was extracted using the Quick-RNA Microprep kit (Zymo) following manufacturer's instructions. 5μl of RNA (roughly corresponding to 1μg) was reverse transcribed to cDNA using the LunaScript RT SuperMix kit - dye based qPCR detection (NEB) following manufacturer's instructions. cDNA was diluted 1:2 with RNAse free water. 1μl of the reverse transcribed cDNA was used in each reaction for qPCR using the Luna Universal qPCR Master Mix (NEB) in a 10μl final reaction in a 384 well plate. 3 technical replicates per sample were measured on a CFX384 Touch Real-Time PCR Detection System (Biorad). Cycles were as follows: 1. Initial denaturation - 95°C, 60s; 2. Denaturation - 95°C, 15s; 3. Extension - 60°C, 30s; Melt Curve - 60-95°C. Steps 2-3 were repeated for 40 cycles. Primers were: IFNB1 FWD - CAGCATCTGCTGGTTGAAGA, RV - CATTACCTGAAGGCCAAGGA; IL6 FWD - CCC CTGACCCAACCACAAAT, RV - ATTTGCCGAAGAGCCCTCAG; GAPDH FWD - GTCTCCTCTGACTTCAACAGCG, RV - ACCACC CTGTTGCTGTAGCCAA. Data was analyzed using the $2^{-\Delta Ct}$ method relative to GAPDH.

Western blot
Cell pellets were lysed in RIPA buffer (Boston Bioproducts) containing cOmplete, Mini, EDTA-free Protease Inhibitor Cocktail (Millipore Sigma) and PhosSTOP (Millipore Sigma) for 10 minutes on ice. Lysates were cleared by centrifugation at 16000g for 10 minutes at 4°C and Laemmli 6X, Sample buffer, SDS, Reducing (Boston Bioproducts) was added prior to loading. Samples were run on NuPAGE 4 to 12%, Bis-Tris Gels (Thermo Fisher) and transferred on nitrocellulose membrane with an iBlot2 (Thermo Fisher). Membranes were blocked in 5% non-fat milk in TBS Tween. Antibodies against phospho proteins were incubated in 5% BSA TBS tween. ECL signal was recorded on a ChemiDoc Biorad Imager. Data were analyzed with ImageLab (Biorad). Antibodies and dilutions are listed in Table S10.

Immunofluorescence for follow-up studies
BJ1 were seeded on Fibronectin bovine plasma coated coverslips at 0.05 million cells/well density in a 24 well plate and stimulated as indicated in figure legends. Cells were then fixed with 2% Paraformaldehyde (Electron Microscopy Sciences) in PHEM buffer (Electron Microscopy Sciences) for 30 minutes at 37°C, washed three times with PBS and quenched with freshly prepared 0.1M Glycine for 10 minutes. Coverslips were then permeabilized and blocked with 10% goat serum (Thermo Fisher) in IF Perm Buffer (PBS, 0.5% BSA (Seracare), 0.05% Saponin from quillaja barka (Sigma)) for 20 minutes. Coverslips were then stained with primary antibodies for 1-2 hours at room temperature in IF Perm buffer supplemented with 10% goat serum, washed 5 times, and then stained with secondary antibodies in IF Perm Buffer for 1-2 hours. Coverslips were then washed 5 times, mounted with Fuoromont-G, with DAPI (Thermo Fisher) and dried at 37°C for one hour. Images were acquired on an Olympus IX83 using an Olympus PlanApo N 60X 1.42NA oil immersion objective controlled by Fluoview software.

Image quantification for VPS52 and RIC1 Arrayed Knockout Experiments
CellProfiler version 4.2.5 was used to extract image-based features from 3 to 5 fields of view and three individual experiments per condition. GM130-positive areas were identified using the IdentifyPrimaryObjects module using the three-class Otsu thresholding method. Objects closer than 30 pixels were merged using the SplitOrMergeObjects module and the objects with an area smaller than 600 pixels were filtered out using the FilterObjects module. STING intensity within the GM130-positive objects was measured using the MeasureObjectIntensity module.

OPS Library cloning, lentivirus production, transduction, and next generation sequencing of libraries
Libraries were cloned as previously described into a CROP-seq-puro-v2 (Addgene #127458) backbone. Lentivirus was then produced and transduced as previously described.[24] For library transductions, multiplicity of infection was estimated by counting colonies after sparse plating and antibiotic selection. Genomic DNA was also extracted for NGS validation of library representation. Genomic DNA was extracted using an extraction mix as previously described.[24] Barcodes and sgRNAs were amplified by PCR from a minimum of 100 genomic equivalents per library using JumpStart 2X Master Mix (initial denaturation for 5 minutes at 98°C, followed by 28 cycles of annealing for 10 s at 65°C, extension for 25 s at 72°C, and denaturation for 20 s at 98°C).

STING stimulation, phenotyping, and in situ sequencing for genome-wide optical pooled screen

HeLa-TetR-Cas9 cells were transduced with pTRIP-hPGK-Blast-2A-STING-mNeonGreen and flow sorted twice to select cells with similar levels of reporter expression. Overexpression of STING was used to maximize the number of proteins that we could image with conventional antibody staining. We selected the hPGK promoter for STING expression based on previous optimization work performed in Gentili et al.[8] Expression from hPGK leads to low levels of STING protein that is degraded at similar levels to WT STING when cells are stimulated with STING agonists. Cells were maintained on blasticidin (20 μg/mL) for 4 days prior to transduction. For screening, cells were selected with puromycin (1 μg/mL) for 3 days after transduction and library representation was validated by NGS. Cas9 expression was induced with 1 μg/mL doxycycline for 1 week and cells were then seeded in six 6-well glass-bottom dishes at 415,000 cells/well 48 hours prior to fixation. cGAMP (Invivogen tlrl-nacga23) was added at 2 μg/mL for 10 minutes at 37°C in cGAMP Perm Buffer (50 mM HEPES (Corning), 100 mM KCl (Thermo Fisher), 3 mM MgCl2 (Thermo Fisher), 0.1 mM DTT (Thermo fisher), 85 mM Sucrose (Thermo Fisher), 0.5 mM ATP (Cayman chemicals), 0.1 mM GTP (Cayman Chemicals), 0.2% BSA (Seracare), 0.001% Digitonin (Promega)). 1mL warm media (DMEM with 10% FBS and 1% Pen-Strep) was then added to each well, media was quickly removed, and 2mL/well fresh media added for four hours prior to fixation. Cells were fixed by removing media and adding 4% paraformaldehyde (Electron Microscopy Sciences 15714) in PBS for 30 minutes at room temperature.

Cells were then permeabilized with 100% methanol for 20 minutes. The permeabilization solution was then carefully exchanged with PBS-T wash buffer (PBS + 0.05% Tween-20) by performing six 50% volume exchanges followed by three quick washes. The sgRNA sequence was reverse transcribed in situ overnight at 37°C using 1x RevertAid RT buffer, 250 μM dNTPs, 0.2 mg/mL BSA, 1 μM RT primer with LNA bases -A+CT+CG+GT+GC+CA+CT+TTTTCAA -, 0.8 U/μL Ribolock RNase inhibitor, and 4.8 U/μL RevertAid H minus reverse transcriptase in 750 μL/well as previously described.[24] After reverse transcription, cells were washed 5x with PBS-T and post-fixed using 3% paraformaldehyde and 0.1% glutaraldehyde in PBS for 30 minutes, followed by washing with PBS-T 3 times.

Cells were stained with primary antibodies for GM130 (1:1300, Cell Signaling Technology Cat# 12480, RRID:AB_2797933) and p62 (1:300, Cell Signaling Technology Cat# 88588, RRID:AB_2800125) in 3% BSA (VWR Cat# 97061-422) in PBS for 4 hours. Samples were then washed 3x in PBS-T for 3 minutes, and incubated with secondary antibodies: 1:1800 donkey anti-mouse antibody (Jackson ImmunoResearch Labs Cat# 715-006-151, RRID:AB_2340762) disulfide-linked to Alexa Fluor 594 (Thermo Fisher A10270) via a custom conjugation, 1:1800 donkey anti-rabbit antibody (Jackson ImmunoResearch Labs Cat# 711-006-152, RRID:AB_2340586) disulfide-linked to Alexa Fluor 647 (Thermo Fisher Scientific A10277) via a custom conjugation, in 3% BSA for 2 hours at 37°C. Finally, cells were washed 6x in PBS-T, and stained with BV421-conjugated anti-CD63 (1:1000, BioLegend Cat# 353029, RRID:AB_2687003). Cells were then imaged and Alexa Fluor 594 and 647 antibodies were destained with 50mM TCEP in 2x SSC for 45 minutes at room temperature. Subsequently, samples were incubated in a padlock probe and extension-ligation reaction mixture (1x Ampligase buffer, 0.4 U/μL RNase H, 0.2 mg/mL BSA, 100 nM padlock probe - /5Phos/GTTTCAGAGCTATGCTCTCCTGTTCGC CAAATTCTACCCACCACCCACTCTCCAAAGGACGAAACACCG -, 0.02 U/μL TaqIT polymerase, 0.5 U/μL Ampligase and 50 nM dNTPs) for 5 minutes at 37°C and 90 minutes at 45°C, and finally washed 2 times with PBS-T. Circularized padlocks were amplified using a rolling circle amplification mix (1x Phi29 buffer, 250 μM dNTPs, 0.2 mg/mL BSA, 5% glycerol, and 1 U/μL Phi29 DNA polymerase) at 30°C overnight. DAPI (600 ng/mL) was then added to cells and cells were imaged in the DAPI and STING mNeonGreen channels for alignment to the first round of phenotyping images. Finally, in situ sequencing was performed as previously described using the sequencing primer GCCAAATTCTACCCACCACCCACTCTCCAAAGGACGAAACACCG for 12 cycles.

Secondary optical pooled screens

Genes to target for the secondary screen were manually chosen based on ranking in the optical pooled screen SVMs, the meta-analysis by information content rankings, and adding select genes of interest from the TurboID dataset.[8] hTert-BJ1 (BJ-5ta - CRL-4001) cells from ATCC were used for secondary screening along with HeLa-TetR-Cas9 cells described above.

Prior to screening, BJ1 cells were transduced with Cas9 (Addgene #96924) and selected using 10 μg/mL blasticidin for 7 days. Subsequently, library transduction was performed as described for HeLa cells above without the addition of doxycycline. BJ1 cells were plated for stimulation 5 days post-transduction at 150,000 cells/well and stimulated with cGAMP and buffer at 7 days post-transduction as described above for HeLa cells.

For BJ1 secondary screening, in situ sequencing and antibody staining were performed as described for the HeLa cells but only imaged for one round of immunofluorescence: 200 ng/mL DAPI with 1:100 pSTING Ser366 (Cell Signaling Technology Cat# 19781, RRID:AB_2737062) as the primary antibody detected with 1:900 custom-conjugated donkey anti-rabbit antibody (Jackson ImmunoResearch Labs Cat# 711-006-152, RRID:AB_2340586) disulfide-linked to Alexa Fluor 647 (Thermo Fisher Scientific A10277).

For HeLa cell secondary screening, one round of antibody staining was performed after reverse transcription and post-fixation, using p62 mouse (1:250, Cell Signaling Technology Cat# 88588, RRID:AB_2800125) for two hours followed by 1:900 anti-mouse antibody (Jackson ImmunoResearch Labs Cat# 715-006-151, RRID:AB_2340762) disulfide-linked to Alexa Fluor 594 (Thermo Fisher A10270) via a custom conjugation for 1 hour and imaged in 200ng/mL DAPI in 2X SSC. Cells were then imaged and the Alexa Fluor 594 antibody was destained with 50mM TCEP in 2x SSC for 45 minutes at room temperature. Subsequently, samples were incubated

in a padlock probe and extension-ligation reaction mixture and amplified using rolling circle amplification as described above. Following 7 cycles of in situ sequencing, HeLa cells were iteratively assayed using 4i[43] for 4 additional imaging cycles (see below):

	Primary Antibody				Secondary Antibody			
Cycle	Antibody	Dilution	Vendor Catalog #	RRID	Antibody	Dilution	Vendor Catalog #	RRID
1	p65	250	Cell Signaling Technology Cat# 6956	RRID:AB_10828935	Anti-mouse AF555+	1000	Thermo Fisher Scientific Cat# A32773	RRID:AB_2762848
	GM130	1000	Cell Signaling Technology Cat# 12480	RRID:AB_2797933	Anti-rabbit AF647+	1000	Thermo Fisher Scientific Cat# A32795	RRID:AB_2762835
2	Actin	1800	Cell Signaling Technology Cat# 3700	RRID:AB_2242334	Anti-mouse AF555+	1000	Thermo Fisher Scientific Cat# A32773	RRID:AB_2762848
	HGS	800	Cell Signaling Technology Cat# 15087	RRID:AB_2798700	Anti-rabbit AF647+	1000	Thermo Fisher Scientific Cat# A32795	RRID:AB_2762835
3	gH2AX	600	Millipore Cat# 05-636	RRID:AB_309864	Anti-mouse AF555+	1000	Thermo Fisher Scientific Cat# A32773	RRID:AB_2762848
	Calnexin	900	Abcam Cat# ab22595	RRID:AB_2069006	Anti-rabbit AF647+	1000	Thermo Fisher Scientific Cat# A32795	RRID:AB_2762835
4	EEA1	200	BD Biosciences Cat# 610456	RRID:AB_397829	Anti-mouse AF555+	1000	Thermo Fisher Scientific Cat# A32773	RRID:AB_2762848
	ATP6V1D	1000	Abcam Cat# ab157458	RRID:AB_2732041	Anti-rabbit AF647+	1000	Thermo Fisher Scientific Cat# A32795	RRID:AB_2762835

To perform iterative fluorescence, after antibody staining and imaging, stripping of fluorescence signal was performed similarly to what was previously described.[43] Briefly, after imaging samples were washed six times quickly in distilled water. Water was then carefully aspirated and elution buffer (previously described) was added to the sample with shaking at 300 rpm for 30 minutes. Samples were imaged in imaging buffer as previously described[43] with the addition of 50 mM HEPES and pH was adjusted to 7.4.[66]

Fluorescence microscopy

All in situ sequencing images were acquired using a Ti-2 Eclipse inverted epifluorescence microscope (Nikon) with automated XYZ stage control and hardware autofocus. The Lumencor CELESTA Light Engine was used for fluorescence illumination and all hardware was controlled using NIS elements software with the JOBS module. In situ sequencing cycles were imaged using a 10X 0.45 NA CFI Plan Apo λ objective (Nikon MRD00105) with the following filters (Semrock) and exposure times for each base: G (546 nm laser at 40% power, emission 575/30 nm, dichroic 552nm, 200 ms); T (546 nm laser at 40% power, emission 615/24 nm, dichroic 565 nm, 200 ms); A (637 nm laser at 40% power, emission 680/42 nm, dichroic 660 nm, 200 ms); C (637 nm laser at 40% power, emission 732/68 nm, dichroic 660 nm, 200 ms).

For the genome-wide primary screen, phenotyping images were acquired using a 20X 0.75 NA CFI Plan Apo λ objective (Nikon MRD00205) with the following filters (Semrock unless otherwise noted) and exposure times: CD63 (405 nm laser at 10% power, Chroma Multi LED set #89402, 30ms), DAPI (405 nm laser at 5% power, Chroma Multi LED set #89402, 10ms), STING mNeonGreen (477 nm laser at 30% power, Chroma Multi LED set #96372, 200ms), AF594 (546 nm laser at 80% power, emission 615/24 nm, dichroic 565 nm, 400ms), AF647 (637 nm laser at 30% power, emission 680/42 nm, dichroic 660 nm, 100ms). Two z-stacks 1.5 μm apart were acquired and images were max-projected.

For the secondary screen, phenotyping images for HeLa cells were acquired using a 40x 0.95 NA CFI Plan Apo λ objective (Nikon MRD70470) with the following filters and exposure times: DAPI (405 nm laser at 100% power, Chroma Multi LED set #89402, 100ms), AF594 p62 (546 nm laser at 100% power, Chroma Multi LED set #89402, 100ms), and STING mNeonGreen (477 nm laser at 100% power, Chroma Multi LED set #96372, 100ms). Subsequent rounds after in situ sequencing were imaged for DAPI, AF555, and AF647 with the same filter sets and laser lines noted above for DAPI, AF594, and AF647, respectively, with the following laser powers and exposure times at 100% power: Cycle 1 - 1/10/10ms; Cycle 2 - 1/5/10/ms; Cycle 4 - 1/30/30ms; Cycle 4 - 4/20/30ms.

Phenotyping images for BJ1 cells were acquired using a 20X 0.75 NA CFI Plan Apo λ objective (Nikon MRD00205) with the following filters and exposure times: DAPI (405 nm laser at 100% power, Chroma Multi LED set #89402, 4ms), and AF647 (637 nm laser at 100% power, Chroma Multi LED set #89402, 40ms). Two z-stacks 1.5 μm apart were acquired and max-projected.

Phosphorylated STING flow cytometry screen

See Liu et al.[12] RFP-LC3B FIP200 KO 293T cells were transduced with pTRIP-PGK-Blast-P2A-STING-HA and selected with 20 μg/mL blasticidin (Thermo Fisher Scientific #A1113903). For screening, 200M RFP-LC3+ STING-HA+ FIP200 KO 293T cells were transduced with Cas9-sgRNA all-in-one Brunello library at MOI=0.4 and selected with 2 μg/mL puromycin for 2 days. 8 days after transduction, 200M transduced cells were treated with 1 μM diABZI (Invivogen, #tlrl-diabzi) for 2.5hr, and then permeabilized with 1X perm buffer (PBS with 0.05% saponin and 0.1% glycine) for 4 min (18). Permeabilized cells were then washed with 1X PBS, and fixed, permeabilized further, and stained using BD Cytofix/Cytoperm kit (#554714) following staining with anti-Phospho-STING (Ser366) (D8K6H) Rabbit mAb (Alexa Fluor® 488 Conjugate) (CST, #41622) and anti-HA Alexa647 (Biolegend, #682404) at 1:200 dilution.

QUANTIFICATION AND STATISTICAL ANALYSIS

Image analysis

Images of cellular phenotype and in situ sequencing of perturbations were manually aligned during acquisition using nuclear masks to calibrate the plate position to each of the four corner wells of a 6-well plate. For the genome-wide screen, images between phenotyping cycles were aligned using masks generated using the STING mNeonGreen channel. Alignment was subsequently refined computationally via cross-correlation of DAPI signal between imaging acquisitions. Nuclei and cells were detected and segmented as previously described and in situ sequencing read calling was performed as previously described.[67] Data analysis functions were written in Python, using Snakemake for workflow control.[68] Image analysis code is available on GitHub. Briefly, for segmentation of phenotyping images from the primary screen, nuclei were segmented using the following parameters: using the following parameters: nuclei smooth = 1.15, nuclei radius = 15, nucleus area 110-1600, DAPI intensity threshold = 6100. Cells were segmented using signal in the GM130 channel, at an intensity threshold = 2800. For segmentation of in situ sequencing images from the primary and secondary screens, nuclei were segmented using the following parameters: nuclei smooth = 1.15, nuclei radius = 15, nucleus area 20-800 (BJ1), 20-400 (HeLa), DAPI intensity threshold = 1500 (BJ1), 2000 (HeLa). Cells were segmented using signal in the four sequencing channels at intensity thresholds adjusted for each plate, between 3800 and 4200. For segmentation of phenotyping images from the secondary screen, nuclei were segmented using the following parameters: nuclei smooth = 25 (BJ1), 9 (HeLa), nuclei radius = 30 (BJ1), 100 (HeLa), nucleus area 700-180000 (BJ1), 200-18000 (HeLa), DAPI intensity threshold = 1900 (BJ1), 1400 (HeLa). All other parameters used for analysis were set to default settings. Background subtraction using a rolling ball algorithm was performed with radius = 50 for all channels in the secondary screen.

Optical pooled screen analysis

Only cells with a minimum of one read matching a barcode in the library were analyzed. For the genome-wide screen, only genes with a minimum of one read matching an sgRNA in the library and 2 sgRNAs with at least 50 cells/sgRNA were considered for analysis. Features were normalized on a per-cell basis relative to cells in the same field of view by subtracting the median and dividing by the MAD x 1.4826.[69] SVM models were trained using the Intel Extension for Scikit-learn[70] and the command svm.LinearSVC(random_state=7, C=1e-5, max_iter = 100000, tol =.00005, class_weight = 'balanced') with an 80/20 train/test split for the perturbed classifier and using all cells for each sgRNA in the unstimulated and increased stimulation classifiers, as these two classifiers were separately pre-trained on non-targeting control cells with the same SVM parameters as the perturbed classifier. Resulting mean model scores were averaged over sgRNAs for a given gene and significance was determined by comparing scores for individual sgRNAs to distributions bootstrapped from non-targeting control cells (bootstrapped 100,000 times). Gene-level p-values were calculated using Stouffer's method to aggregate across sgRNAs targeting the same gene and subsequently corrected using the Benjamini-Hochberg procedure.

Meta-Analysis by Information Content

MAIC scores were calculated for each screen (Table S4) using MAIC version 1.0 with default parameters[27]). Pearson correlations of MAIC scores between different screens are shown in Figure 1I. For each screen, the top 500 genes in each direction (if applicable) significant at p < 0.05 were selected as input except for the TurboID dataset, where the full list of 132 genes significant at p < 0.07 was used as discussed previously.[8]

Dimensionality reduction and clustering

PHATE 1.0.10[34] was used to cluster genes using mean gene-level feature values. For the genome-wide screen, PCA was performed and 31 PCs were selected, preserving 95% of variance in the data. PHATE was then performed using the following parameters: knn_dist = 'euclidean', gamma = 1, knn = 2, random_state = 7). For the secondary screen, PHATE was performed using no PCA prior to clustering, since the dataset was already reduced to 20 features by co-clustering features using hierarchical clustering and taking average values across all features in each cluster. The following parameters were then used for PHATE clustering: knn_dist = 'euclidean', gamma = 0, knn = 1, random_state = 7, mds_dist = 'cosine'. Leiden clustering was also performed. To determine the optimal number of clusters, Leiden clustering was performed at varying resolutions on 90% of the data (selected across 15 iterations) and cluster stability assessed using ARS (sklearn.metrics.adjusted_rand_score)[71] in order to select an optimal resolution parameter for clustering. To identify clusters enriched for hits from our classifiers or significant DEGs from the genome-scale Perturb-seq data,

we used the rank genes groups function in scanpy.[72] Clinvar data containing pathogenic allele annotations was downloaded from the April 30, 2022 release, noted in the key resources table.

Phosphorylated STING flow cytometry analysis

Guide RNA abundances were extracted from FASTQ files using poolq 3.3.2 with fixed row and barcode policies. Resulting log-abundances were then subtracted between sorting bins from each experimental condition and analyzed using the Broad Genetic Perturbation Platform screen analysis tool (https://portals.broadinstitute.org/gpp/public/analysis-tools/crispr-gene-scoring) using a hypergeometric analysis.